AALBORG UNIVERSITY

NANOBIOTECHNOLOGY

MASTER'S THESIS

Emulsion Electrospinning Antibacterial Fibres with a 3D Printed Microfluidic Droplet Generator

---

Author:
Magnus Undall-Behrend
Daugaard

Supervisor:
Peter FOJAN

June 3^{th} 2021

AALBORG UNIVERSITY
STUDENT REPORT

AALBORG UNIVERSITY
STUDENT REPORT

Fifth year at Faculty of Engineering and Science
Nanobiotechnology
Skjernvej 4A
9220 Aalborg
http://www.mp.aau.dk/

Title:

Emulsion Electrospinning Antibacterial Fibres with a 3D Printed Microfluidic Droplet Generator

Project:

Master's Thesis

Project period:

September 2020 - June 2021

Group members:

Magnus Undall-Behrend Daugaard

Supervisors:

Peter Fojan

Number of pages: 47
Appendix: 1
Ended: 3 June 2021

Abstract:

In this project emulsion electrospun fibres were fabricated by direct electrospinning from a 3D printed microfluidic droplet generator. A 20% polyvinylpyrrolidone solution were the continuous phase liquid, a 100 mM tert-butylbenzoquinone in grapeseed oil solution were the dispersed phase liquid. The compartments on the fibre were between 2.855 and 6.564 µm. The diameter of the fibres were between 0.897 and 2.486 µm. Release profiles were made for two samples of emulsion electrospun fibres, two individual patterns were seen. However, an equilibrium determined release were seen for both. The droplets were generated with two different flow rate sets, either the first with, 80 µL/min and 16.5 µL/min or the second with 50 µL/min and 12.5 µL/min, for continuous and dispersed flow, respectively. Droplets produced had average diameters of 0.469 and 0.742 µm with standard deviations of 0.213 and 0.0159 µm for the first and second set, respectively. COMSOL Multiphysics v5.5 2D and 3D simulations of droplet generation produced droplet with diameters of 1.430 and 1.550 µm.

PREFACE

This master's thesis was written by Magnus Undall-Behrend Daugaard as part of the nanobiotechnology programme at Aalborg University. The project spanned a period of 9 months from 02/09-2020 - 3/06-2021. The project was supervised by Lector Peter Fojan.

The project will cover the emuslsion electrospinning of polymers, facilitated by droplet generation in a 3D printed microfluidic droplet generator. COMSOL simulations of the droplet generation will be performed.

Source references throughout the project were written with square brackets and according to the IEEE citation style. References used for specific paragraphs or citations have been listed hereafter. Results or arguments from other studies have been denoted with a reference after the sentence.

LIST OF ABBREVIATIONS

AC	Alternating Current
DC	Direct Current
DLP	Dynamic Light Processing
DMD	Digital Mirror Device
FDM	Fused Deposition Modelling
LCD	Liquid Crystal Display
PAA	Poly(acrylic acid)
PCL	Polycaprolactone
PEG	Poly(ethylene glycol)
PVA	Polyvinyl Alcohol
PVP	Polyvinylpyrrolidone
SLA	Stereolithography apparatus
SLS	Selective Laser Sintering
TBBQ	tert-butylbenzoquinone
UV	Ultraviolet

Contents

CHAPTER 1

INTRODUCTION

Electrospun fibres are interesting in a wide field of application. The tunability and versatility of the fibres enable various applications within, e.g filters, scaffolds, protective clothing, batteries, catalysts, electronics, optics, wound treatment, and antibacterial treatments. The wide variety of applications are due to the highly tune-able properties of electrospun fibre mats. These include mechanical strength, porosity, fibre diameter, and surface composition. [1]–[15] One of the most interesting properties of electrospun fibres is the high surface to volume ratio, which is required for almost all of the aforementioned applications. Therefore, functionalisation of electrospun fibres are of great interest as the high surface to volume ratio will enhance the effect of the functionalisation [16]. There are different ways to functionalise electrospun fibres. One is cross-linking the surface of the spun fibres with a compound. Electrospun polymethylmethacrylate fibres were functionalised with collagen in order to increase the compatibility with the extracellular matrix in order to improve scaffolding potential of the fibres [17]. Even though functionalisation may be favourable for scaffolding it is not required. Pelipenko et. al [18] produced simple polyvinyl alcohol (PVA) fibre scaffolds with varying fibre diameter. It was shown that the fibre diameter was crucial for successful scaffolding, however, it was also shown that different cell lines had different preferences regarding fibre diameter. Gomes et. al [19] produced electrospun fibre mats of polycaprolactone (PCL), chitosan, and gelatine and tested both cell-scaffolding and wound healing properties of the fibre mats. All materials did enable cell proliferation, however, regarding wound healing the chitosan fibres were the most efficient. [14], [16]–[19] Functionalisation of electrospun fibres for wound dressings are of great interest as electrospun fibres generally show great properties related to wound healing. Electrospun fibre mats can show porosity and wetability favourable for wound healing. An asymmetric electrospun fibre mat comprised of a dense PCL layer with a porous chitosan/poly(ethylene oxide) (PEO) layer with Aloe Vera incorporated, have been produced [20]. This design did show mechanical properties similar to native skin, it presented blockage of incoming microorganisms and good wound healing properties due to the incorporated Aloe Vera. Aloe Vera have also been used for wound dressings for burn wounds, where it was electrospun in a fibre mat spun from a polymer blend of poly(vinyl alcohol)/poly(acrylic acid)/poly(ethylene glycol)/poly(vinylpyrrolidone)

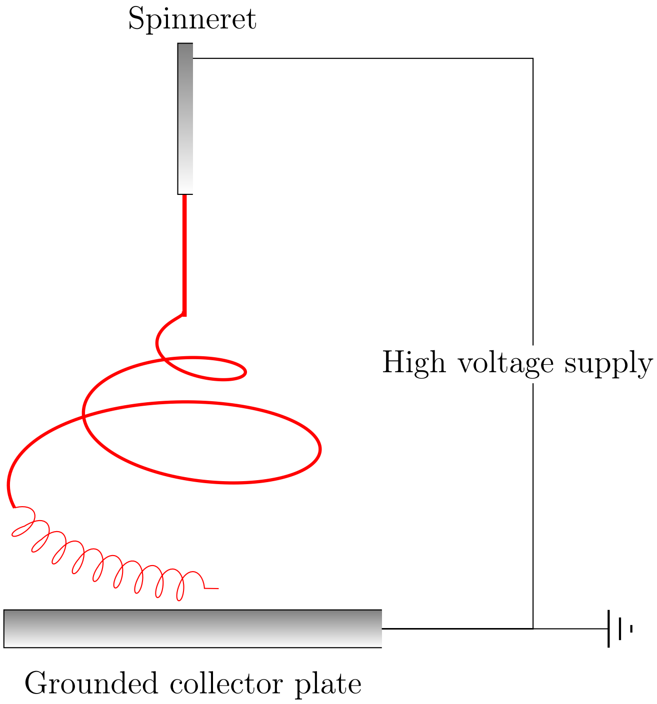

Figure 1.1: Schematic of the electrospinning setup, a high voltage supply connected to a grounded collector plate and the spinneret from which the solution is spun. The solution is supplied by a syringe pump or similar.

(PVA/PAA/PEG/PVP) [1]. Beside aloe vera other compounds can be used to functionalise fibres for wound dressings. Antibacterial fibres will also be favourable for several types of wounds. There have been produced antibacterial wound dressings for prevention of post surgery abdominal infection and adhesion. For these the polymer poly(lactide-co-glycolide) was electrospun with antibiotics incorporated within the fibres. [21]

1.1 Electrospinning of Polymer Solutions

Electrospinning is a versatile method to produce polymer fibres from either a polymer solution or melt. A general electrospinning setup (fig. 1.1) consist of a high potential source, a grounded collector and a spinneret. The spinneret is where the solution or melt is supplied from, the spinneret is often a blunt hypodermic needle. [13], [14], [22]–[25]

There are four steps involved in electrospinning. First, electrostatic charging of the polymer solution will accumulate charges on the surface of the polymer solution, the surface tension will favour a spherical droplet, however when the potential accumulate enough charges, the electrostatic forces will deform the droplet into a Taylor cone. [13], [14], [25], [26] This deformation occur when the electrostatic pressure, (p_e), exceed the

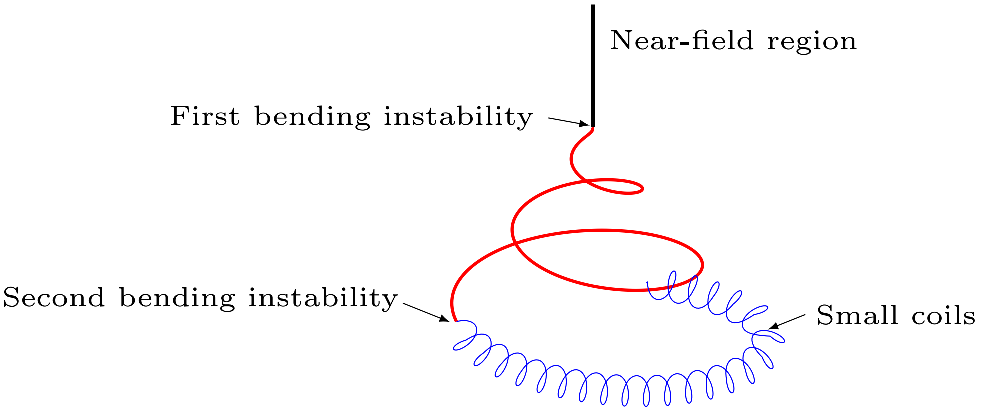

FIGURE 1.2: Schematic of the electrospinning process. The black segment represent the near-field region where the jet propagates in a straight line towards the collector. The red colour indicate the region of the first bending instability, where a conical spiral are produced. The blue colour indicate the region of the second bending instability, where smaller coils are formed within the conical spiral pattern.

capillary pressure, (p_c). The electrostatic pressure is given by:

$$p_e = \frac{\epsilon E^2}{2} \tag{1.1}$$

where ϵ is the dielectric constant of the surrounding medium and E is the electric potential applied. The capillary pressure is given by the Young-Laplace equation:

$$p_c = \frac{2\gamma}{r} \tag{1.2}$$

where r is the mean radius of curvature, which corresponds to inner radius of the spinneret, γ is the surface tension. When the voltage reach a critical voltage, (V_c), p_e will surpass p_c and the electrostatic repulsion will overcome the surface tension. The critical voltage can be calculated by:

$$V_c^2 = \frac{4H^2}{h^2}(ln(\frac{2h}{R}) - 1.5)(1.3\pi R\gamma)(0.09) \tag{1.3}$$

where H is the distance from tip of the spinneret to the collector, h is the length of the spinneret, R is the outer radius of the spinneret, H, h, and R is in cm. γ is in dyn/cm and voltage is kV. The factor 1.3 originate from the geometrical shape of the cone with a semi vertical 49.3°angle at equilibrium [27]. Furthermore, the viscoelastic forces must be overcome in order to deform the droplet and generate the Taylor cone i.e. a too high viscosity prevents formation of the Taylor cone. [14], [25]–[27]

Secondly, a jet of polymer is stretched from the apex of the Taylor cone. Initially the jet will extend in the direction of the electric potential. However, after a certain distance instabilities occur. The first region with straight propagation of the jet is called the near-field region (fig. 1.2). In the near-field region the viscoelastic forces must suppress the Rayleigh instabilities in order to prevent breakup into droplets. Third, the jet will thin as it accelerates, and the surface tension and viscoelastic forces tend to prevent further movement forward, and the acceleration will cease as the jet is thinning. The straight movement can easily be interrupted when the acceleration becomes constant or drops to 0. Such a small change can easily arise from surface charges. When the straight movement is stopped the far-field region is entered and three types of instabilities can occur to the jet. The first type is axisymmetrical, also called Rayleigh instability, which might lead to breakup into droplets. However, at strong enough electric field it may be suppressed. The second type is also axisymmetrical, but occur at a higher potential than the first. The third type, bending instabilities, is non-axisymmetrical and describes the bending of the jet into a conical spiral shape (fig. 1.2), where the elongation occur at a much higher rate due to the increased pathway in the conical pattern. The rapid elongation will also rapidly thin the jet in order to ensure continuity of the jet. After a certain distance a secondary bending instability may occur, where smaller coils are generated (fig. 1.2). Fourth, the solidification of the jet into a fibre occur due to evaporation of solvent. At the point of solidification any instabilities cease even though charges might still be trapped in the polymer. The morphology of the fibres formed are mainly determined by which step of instability the jet reached prior to solidification. For fibres obtained in the first bending instability, it is easy to retrieve fibres on a collector as a fibre mat. However, more complex coils and morphologies can be obtained when entering higher order bending instabilities. The charges trapped in the fibres tend to restrict the thickness of a fibre mat to below one mm. [13], [14], [22]–[25], [28]–[31]

There are three major groups of parameters to regard when electrospinning, these are, solution properties, process parameters, and environmental factors. Solution properties include viscosity, conductivity, polymer concentration, polymer molecular weight, surface tension, and vapour pressure. Process parameters include the applied voltage, the distance from solution to the grounded collector plate, and the flow rate at which the solution is supplied. Environmental factors are humidity and temperature. [24]

The solution properties have the most significant impact on the electrospinning process. During electrospinning beading of the fibre may occur, this beading is the result of surface tension acting upon free polymer molecules in the solution, as it will decrease the area by a spherical shape. However, it is possible to prevent beading by adjusting the viscosity of the solution. The viscosity also represent the molecular entanglement of the polymer, which is dependent on the molecular weight and concentration of the polymer. When the molecular entanglement exceed a critical point formation of fibre becomes possible, as the viscoelastic forces are high enough to prevent Rayleigh instabilities during electrospinning. However, studies have shown that the critical concentration of polymer might not always be purely dependent on the viscosity, as it was shown that the polymer concentration of both 8 kDa and 8 mDa PEO required for fibre formation was the same, even though the viscosity was very different. [2], [3], [22], [24], [32] The viscosity and conductivity of the solution will impact the degree of elongation the fibre can undergo, effectively determining the diameter of the fibre. Furthermore, the viscosity determines how wide an area of the collector the fibres will be collected on, as higher a viscosity will delay the onset of bending instabilities. This delay will decrease the radius of the cone, and thereby also decrease the elongation path which increases the fibre diameter. [2], [3], [22]

1.1.1 Alternative Electrospinning

There exists a variety of different electrospinning techniques other than the conventional approach. One way to produce different fibres are by using AC instead of DC voltage. AC electrospinning is a less popular approach than DC electrospinning, however, AC electrospinning have shown increased production rates for similar electrospinning setups. Drug-loaded fibres spun with AC electrospinning were produced with a polymer blend of PVP and acrylate polymer. [33]

Another way to increase production of fibres is needleless electrospinning. Where the spinneret is removed, and the fibres are produced directly from a reservoir. There will often be a constantly wetted geometry which will have edges where several Taylor cones will occur simultaneously. These geometries can include, balls, beaded chains, discs, or spiral coil spinnerets which are constantly in contact with a solution reservoir in order to facilitate continuous fibre generation. [14], [24], [34]

Another approach to alternative electrospinning is modifying the spinneret. Different spinneret geometries will result in different fibre generation. If the spinneret in fact split up the polymer jet multi-jet electrospinning is achieved, the same tendency can be achieved by an array of needles. [14], [24], [35] Centrifugal electrospinning can be used to produce more aligned fibres, at a high production rate. However, fibres produced by centrifugal electrospinning, might be difficult to maintain continuous due to the stretching of fibres. [14], [36]–[39]

Co-Axial Electrospinning

Another type of spinneret is the co-axial needle setup, where two liquid are electrospun at once, a core and a shell liquid. These two phases are immiscible, and often will the core liquid not be able to electrospin by itself. The spinneret is build like two concentric channels, one inside the other just before the end of the outer tube the inner tube stops, and creates a co-flow of the two liquid phases (fig. 1.3). The process parameters

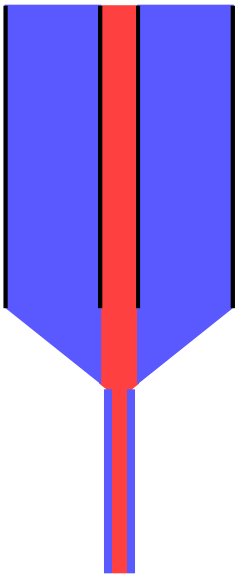

FIGURE 1.3: Schematic of the a co-axial electrospinning spinneret. The blue phase is the shell polymer and the red phase is the core solution.

regarding electrospinning are especially important for co-axial electrospinning, as the right flow rate are required for both phases.

The core-shell configuration of the electrospun fibres are of interest as encapsulation of components in the core phase are possible. This encapsulation will enable further possibilities within tissue engineering and drug delivery systems. The incorporation of a compound might enable a higher resemblances to the extracellular matrix, which is required for successful tissue engineering. By combining the mechanical strength of poly(lactic-co-glycolic acid) and Nerve growth factor, an implant which promotes nerve regeneration were electrospun by co-axial electrospinning. [40]–[43]
The incorporation of a drug in the core can enhance release profiles from the fibre, however, not all shell layers will have the same effect on the release. The shell are often needed to counter the initial burst release of drug in drug delivery systems. If the initial burst release are rapid enough the concentration might exceed the minimum toxic concentration, which should be avoided. Therefore, a successful reduction of burst release is needed to provide a sustained drug release. Some systems will provide such release profiles, while other will not. If the core phase remains liquid a breakage of the fibres might be the reason for this, as the core will flow freely from the fibre. This free flow might be countered by emulsion electrospinning as individual compartments of the core phase is produced. [43]–[47]

Emulsion electrospinning

Emulsion electrospinning is when the electrospun solution contains emulsions. The emulsions can be produced by various methods the only requirement, however, is that

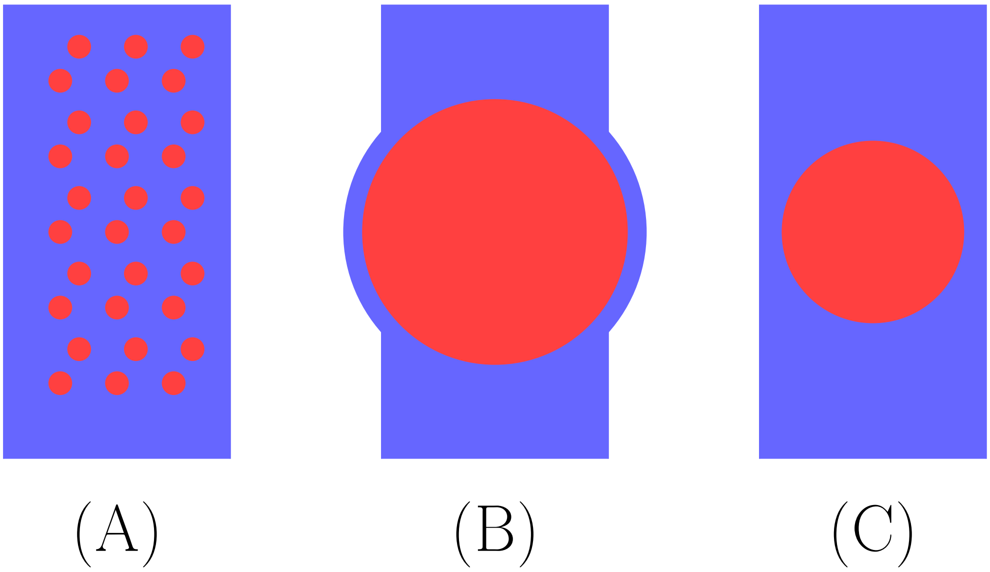

Figure 1.4: Schematic of emulsion electrospun fibres. The blue phase is the shell polymer and the red phase is the core solution. In (A) small droplets are randomly distributed. In (B) a spindle-like fibre occur as the droplet have a larger diameter than the fibre. In (C) a droplet just little smaller than the fibre are located in the centre of the fibre.

the emulsion must be stable, as the emulsion should not coalesce before the solution is electrospun. When emulsion electrospinning, the properties of the emulsion are important when considering the resulting fibre. There are generally three fibre types produced by emulsion electrospinning. The first is the presence of many small droplets encapsulated at random locations within the fibre (fig. 1.4a). The second is the presence of a large spindle-like droplet which widen the fibre, as the droplet are larger than the fibre (fig. 1.4b). The third is a larger droplet which still does fit within the fibre, and does not widen it (fig. 1.4c). [14], [24], [40], [42], [43]

Sustained release of the two different proteins bovine serum albumin and nerve growth factor from electrospun fibres with poly(l-lactide-co-ϵ-caprolactone) as the outer phase, these fibres were of the first fibre type with small droplets [47], [48].
A new approach to emulsion electrospinning could be unstable emulsion electrospinning, where the emulsion must be electrospun shortly after generation. When looking at different ways to produce emulsions, the one best suited for such live generation must be microfluidic droplet generation. Microfluidic droplet generation, enable a sustained production of monodisperse droplet. Furthermore, it should be possible to connect such a microfluidic droplet generator to an electrospinning setup.

1.2 Microfluidic Droplet Generation

An easy way obtain emulsions are by microfluidic droplet generation. The breakthrough in microfabrication in the 1980's have allowed vast applications of microfluidics. Microfluidics regard the flow of fluids inside devices with channels in the micrometer range, which have the advantage of low volume consumption. Due to the minimisation the flow in a microfluidic device is different than conventional flows. With the increase in area to volume and surface area related parameters such as, pressure, shear forces, and surface tension become more dominant. [49]–[51]

1.2.1 Dimensionless Numbers

The forces regarding microflow are governed by the Navier-Stokes equations. These forces are inertial, viscous, capillary, and gravitational forces. It is possible to unify these forces. When considering a volume of fluid with velocity u in a microfluidic device with length L. Then the intertial stress will go as $f_i \sim \rho u^2$, viscous stress $f_v \sim \mu u/L$, gravity $f_g \sim \rho g L$, and capillary pressure $f_\gamma \sim \gamma/L$. Based on these connections several dimensionless numbers, which can be useful to describe microflows, can be calculated. In principle the ratio between any of these connections defines such a dimensionless number. The Reynolds number is the ratio between inertia and viscous force $Re = f_i/f_v$,

$$Re = \frac{\rho u L}{\mu}. \tag{1.4}$$

The Reynolds number will usually describe if a flow is laminar or turbulent. However, for microfluidic devices L is usually small and Re will be small. This indicate that viscous stress dominate inertia, giving laminar flow. For two-phase flow Re is rarely used.

For microfluidics the capillary number Ca is more commonly used, it is the ratio between viscous stress and capillary pressure $Ca = f_v/f_\gamma$,

$$Ca = \frac{\mu u}{\gamma}. \tag{1.5}$$

Both viscous and capillary forces are enhanced when L becomes smaller, this indicates that inertia and gravitational forces are smaller than those in a microfluidic device. [49], [50]

1.2.2 Droplet Generation

The generation of droplet occur due to fluidic instabilities. In microfluidic devices such instabilities, are readily produced, which in turn enable droplet generation. As droplet generation requires immiscible liquid, there will often be an organic hydrophobic phase with an aqueous hydrophillic phase. However, as the interfacial tension between the two phases are important a surfactant might be required in order to prevent coalescence. There are several modes by which droplet generation can occur, the most observed three modes are, dripping, squeezing, and jetting. Dripping and jetting originate from capillary instabilities which arise from interfacial tension forces which act to reduce the interfacial energy. For these modes the viscous and inertial forces seek to deform the liquid interface, which is counteracted by the interfacial tension forces. The balance of these forces determine which mode of droplet generation are seen. However, for squeezing the channel confinement are also among the dominant parameters. [50], [52] The geometry of the microfluidic device will impact the droplet generation. Some commonly used microfluidic droplet generation geometries have either co-flow (fig. 1.5a), cross-flow (fig. 1.5b), or flow-focusing (fig. 1.5c) geometries.

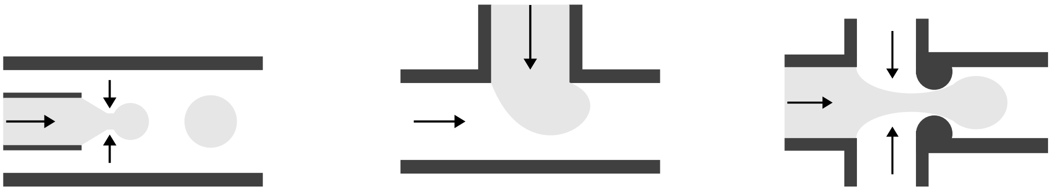
(A) (B) (C)

FIGURE 1.5: Schematic of microfluidic device geometries. The continuous phase is white and the dispersed phase is grey. (A) Co-flow geometry. The continuous phase flow around a inner channel which supplied the dispersed phase in the same direction the continuous phase will breakup droplets. (B) Cross-flow geometry. The continuous and dispersed phase flow will cross each other and form droplets. (C) Flow-focusing geometry. The continuous phase is used to narrow the stream of dispersed phase until it breaks off.

In the cross-flow geometry (fig. 1.5b) the droplet can be generated by two different mechanisms. The first is where the droplet rapidly fill the junction region and become confined by the channel walls. The second is where droplet breakup occur before the droplet fill the channel. The confined droplet breakup occur when the size of the continuous phase channel and dispersed phase channel are of comparable size. For this confined breakup, an additional force act on the droplet, as it acts as a plug in the channel and a pressure buildup occur. The continuous phase flow rate determines how large the plug grows before droplet breakup. The unconfined droplet breakup occur, when the dispersed phase channel is significantly smaller than the continuous phase channel. For this type of droplet breakup, the factor most dominant for droplet size is the continuous phase flow rate. Cross-flow geometries generally produce monodisperse droplets with coefficient of variation below 2%.

In co-flow geometries (fig. 1.5a) droplet are pinched off a stream of dispersed phase, the interfacial tension acts to keep the droplet at the end of the inner channel. The continuous phase flow rate must exceed a certain level in order to induce pinch off.

In the flow focusing geometries (fig. 1.5c) the breakup is induced directly by the continuous phase. As the dispersed phase blocks the narrow outlet, the continuous phase are focused and accelerated around the dispersed phase, thus exerting a large pressure. This pressure will press the two liquid interfaces together, when they touch the droplet will break off.

The geometry is the most important factor of the microfluidic droplet generator. However, the wettability of the channel walls also have an impact on the droplet generation. The walls should preferably be wetted with the continuous phase, in order to ensure that there always are a shell around the dispersed phase. If the dispersed phase wets the wall better than the continuous phase, irregular two-phase flow will occur, and monodisperse droplet generation will become difficult. [50], [52], [53]

Passive and Active Droplet Generation and Breakup Modes

There are two ways to achieve droplet generation in microfluidic devices either passive or active droplet generation. In both cases the two-phase flow is controlled by pumps which supply a constant flow rate or pressure regulators which keep a constant pressure on the fluids. During passive droplet generation only the forces contributed from the liquid movement are responsible for droplet generation. However, for active droplet generation an extra energy source is introduced, it could be vibrations or electric fields. [52], [53]

The three primary breakup modes, dripping, squeezing, and jetting all have different characteristics. Droplets generated by squeezing are larger than the channel dimension, with a high degree of monodispersity. Droplets generated by dripping are smaller than the channel dimension and also monodisperse. Jetting also produce droplets smaller than the channel dimension, but are often polydisperse. The same geometry can produce droplets by all three breakup modes, the continuous phase capillary number, can be used to describe regimes for each mode. However, the different geometries might favour one breakup mode over the rest, due to the different effects which facilitate droplet breakup. Squeezing breakup tend to occur at low capillary numbers in microfluidic devices. The shear forces becomes significantly smaller than the interfacial forces. Therefore, will the droplet increase in size and plug the channel and a pressure buildup will occur prior to droplet breakup (fig. 1.6).

When the capillary number increases the squeezing will go to dripping. In the dripping regime the viscous forces increase to a point where the interfacial tension forces are overcome and droplet breakup occur. However, the interfacial tension will stabilise the emerging droplet against further breakup. If the viscous stress are constant, highly monodisperse droplets are generated (fig. 1.6). In the transition between squeezing and dripping a intermediate breakup where both viscous forces and build up pressure facilitate droplet breakup.

When the capillary number increases further jetting will occur. In jetting an extended liquid jet protrude from the dispersed phase channel. This jet will at some point break up into droplets due to Rayleigh-Plateau instabilities, when the jet reach a critical length (fig. 1.6). This breakup occur due to interfacial tension and energy minimisation. Jetting tend to produce less monodisperse droplets compared to squeezing and dripping. [50], [52]–[55] It is evident that microfluidic droplet generation are dependent on the flow rates and capillary number, hence also viscosity and interfacial tension. Therefore, several parameters impact the morphology of the produced droplets.

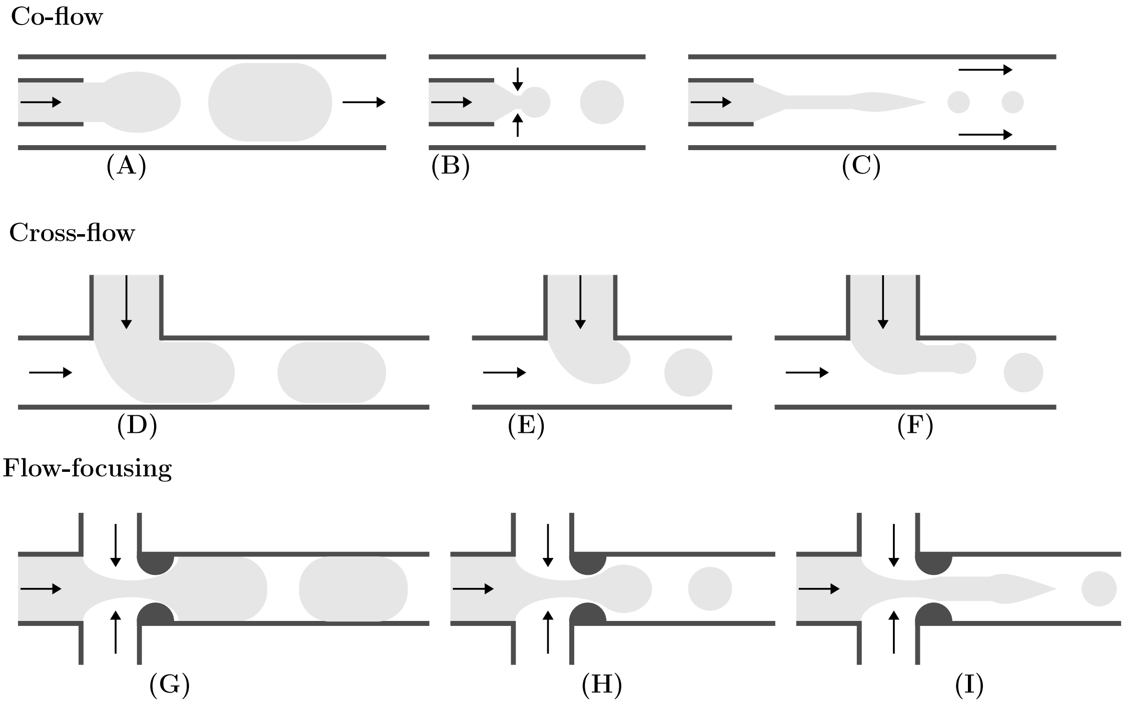

FIGURE 1.6: The different droplet breakup modes. (A)-(C) show squeezing, dripping, and jetting, respectively, in a co-flow geometry. (D)-(F) show squeezing, dripping, and jetting, respectively, in a cross-junction geometry. (G)-(H) show squeezing, dripping, and jetting, respectively, in a flow-focusing geometry. The white colour represent the continuous phase and the grey colour represent the dispersed phase

As the breakthrough in microfluidics started when lithographic methods were developed, these are the most common way to manufacture such devices. However, lithographic methods often require custom made masks, which is time consuming to produce for each individual design. Recent progress in 3D-printing techniques have enabled fabrication of microfluidic devices, such as droplet generators. By 3D-printing different designs can be prototyped fast and easily. [52], [56]–[59]

1.3 3D Printing

When considering 3D printing as a method of fabricating microfluidic droplet generators it is important to evaluate which 3D printing method is best suited for production of such devices. 3D printing can be done from several starting materials, common for all is the principle of additive manufacturing (Bottom up), where the geometry is build up from smaller components. Within 3D printing the small components can be molten thermoplastics, powder or liquid UV-resin. With fused deposition modelling (FDM) a molten thermoplastic is supplied through a nozzle, which then deposits the material layer by layer in a predetermined pattern. The resolution of this method depend on the nozzle size and the thermoplastic used. Powder can be applied for selective laser sintering (SLS), where a laser initiate fusing of the powder into a solid layer. For liquid UV-resins light are used to cure the resin, this can be done with a stereolithography apparatus (SLA), which scan an UV-laser across the resin chamber, the vat, which then produces the image layer by layer. An improved method of SLA is digital light processing (DLP), where a digital micromirror device (DMD), liquid crystal on silicon or liquid crystal display (LCD) is introduced. The DMD consists of thousands micromirrors which can either be in on or off position, thus acting as pixels, either allowing light to pass through or not. Therefore, the DMD is an dynamic mask which enable precise exposure of a whole layer at one time, compared to methods scanning each pixel of the layer one at a time, thus reducing printing time drastically. However, by introducing this the resolution depends on the DMD or LCD rather than the light source. Another method involving UV-reins are inkjet printing, where the resin in jetted at the surface, and the cured by an UV-light source. The methods using UV-resin often produce higher resolution prints. However, for commercially available tabletop printers the minimum feature should not surpass 500 µm as features below this limit often contain artefacts. These artefacts occur as proper cleaning of supporting material within the channels are difficult, as the best solvent also dissolve the solid material. If a weaker solvent such as isopropanol are used, a long exposure should be avoided, as swelling and deformation of the channel might occur. [57]–[59]

The real domain of microfluidics is channel sizes below 100 µm, however, such dimensions are rarely produced by commercial 3D-printing setups. These are often in dimensions between 500 µm and a few mm [57]–[59]. The lack of real microfluidic channel does, however, not make such devices useless. Devices with channel widths above 1 mm have still been used for various microfluidic applications [52], [57]–[59]. Droplet generators with both cross-flow, co-flow and flow-focusing geometries have been 3D-printed. A common thing to consider with 3D-printed channels are the wettability of the channel wall, as this can have an impact on the droplets generated, if the dispersed phase have better wetting properties than the continuous phase. For

3D-printed channels the texture of the walls are one thing that are hard to control, rugged walls are common and can alter the wetting properties drastically. Therefore, 3D-printing is a suitable way to produce microfluidic droplet generators, even tough, some considerations have to be made. [52], [57]–[59]

In this project emulsion electrospun fibres will be produced by electrospinning directly from a 3D-printed microfluidic droplet generator device. The emulsion will contain tert-butylbenzoquinione (TBBQ), an antioxidant, and release profiles from the electrospun fibres will be measured by fluorescence spectroscopy.

Chapter 2

Method and Materials

In order to fabricate emulsion electrospun fibres, a microfluidic droplet generator should be produced. In this project such generators were produced by resin 3D-printing.

2.1 Fabrication of 3D-Printed Microfluidic Droplet Generators

Various designs for a 3D-printed microfluidic droplet generator were prototyped with an Anycubic Photon DLP resin printer (Model: Anycubic photon-5.5). The printer utilises DLP printing techniques with a dynamic LCD Shadow Mask. XY resolution of 47 µm, corresponding to 2560x1440 pixel, and a z-axis accuracy of 1.25 µm. It has an integrated 25 W UV-LED light source at 405 nm. The printing volume is 115 mm x 65 mm x 155 mm, and the resin used should be 405 nm UV resin. Suggested layer thickness is between 25 and 100 µm. Various settings were tested in order to achieve a perfect amount of exposure, that would produce open microfluidic channels. The UV-resin used was either PrimaCreator Value Standard Clear UV-Resin or PrimaCreator Value Water-washable UV-resin. Normal exposure should be between 4-8 seconds as prescribed by the manufacturer. However values between 4.5-9 seconds were tested. After initial testing all printing was done with the same settings (table 2.1). After printing the channels were blown out with nitrogen, then the channels and exterior were washed with the appropriate solvent, either isopropanol or deionised water. After washing the print was dried with nitrogen, followed by 2 minutes curing in an Anycubic Wash&Cure machine. The Anycubic Wash&Cure was also used for washing in isopropanol. After proper cleaning the prints were coated with clear nail polish in

Table 2.1: The optimised printing settings for 3D-printing of the microfluidic droplet generators.

Parameter	**Value**
Normal exposure time	6.5 seconds
Bottom layers	8
Bottom layer exposure	70 seconds
Layer Thickness	50 µm
Lift-off time	7 seconds

order to increase transparency, which increased the visibility of the produced droplets. 3D-files were made in AutoDesk Inventor 2021, and saved as .STL files, which the slicer software CHITUBOX can process into a .photon file, which the printer can recognise and print.

2.2 Conventional Electrospinning

Before the droplet generators were tested for emulsion electrospinning, a set of polymer solutions were tested. This was done in order to establish which polymers were able to be electrospun as pure polymer fibres. A table of the different polymers can be seen in (table 2.2). The electrospinning setup was comprised of a high voltage power supply (Glassman High Voltage, INC. Model:PS/MJ30P0400-22), a grounded metal collector plate, with adjustable height, a mount for the needle, and a syringe pump (New Era Pump Systems Model NE-1010). The tip-collector distances tested varied between 8 and 24 cm dependent on the polymer. The voltages tested varied between 9 and 30 kV. The temperature varied between 20-22 °C and the relative humidity varied between 12-78%.

Table 2.2: List of the different polymers, their molecular weight and lot numbers. The chemicals are purchased from Sigma Aldrich unless otherwise stated.

Polymer	Molecular Weight	Lot Nr.
Carboxymethyl cellulose	250 kDa	07813CH
Polyethylene oxide	300 kDa	MKBF8404V
Polyethylene oxide	5000 kDa	MKAA1971
Starch	N/A	80K1147
Polyvinylpyrrolidone	360 kDa	118K0006
Polyvinylalcohol	89-98 kDa	MKBH1410V
Polyvinylalcohol	72 kDa	Q2901 [Kem-En-Tech]]
Poly ethylene co vinyl alcohol	44 mol% ethylene	MKBF9508V
Polycaprolactone	80 kDa	MKCG2051
Polyvinylidene fluoride	275 kDa	MKBS7583V
Cellulose acetate	30 kDa	MKBQ2122V
Gelatine	N/A	N/A

2.3 Droplet Generation

The two-phase system used for droplet generation consisted of a polymer solution as the continuous phase and grapeseed oil (GSO) as the dispersed phase. In order to increase the visibility of the droplets Nile Red were added to the GSO. The solutions were supplied through two syringe pumps either (New Era Pump Systems Model NE-1010) or (Harvard Apparatus Programmable PHD 2000) the latter were also be used for systems where two dispersed phases were supplied. The diameter of the droplets produced were analysed by ImageJ with images captured by a SEM (Zeiss EVO 60).

2.4 Numerical simulation of Droplet Generation

Numerical simulations of droplet generation was made both in 2 and 3 dimensions in COMSOL Multiphysics v5.5. The geometry was a simple T-junction as produced by 3D-printing. The simulation was performed on a T-junction with rectangular channels where the continuous phase was in a 1x1 mm channel and the dispersed phase was in a 0.75x0.75mm channel (fig. 2.1). The 2D model were built with mesh setting finer, which equals 24862 domain elements. The 3D model were built with mesh setting coarse, which equals 89037 domain elements. The length of the main channel for the 2D model were 14mm whereas it was 10mm for the 3D model.

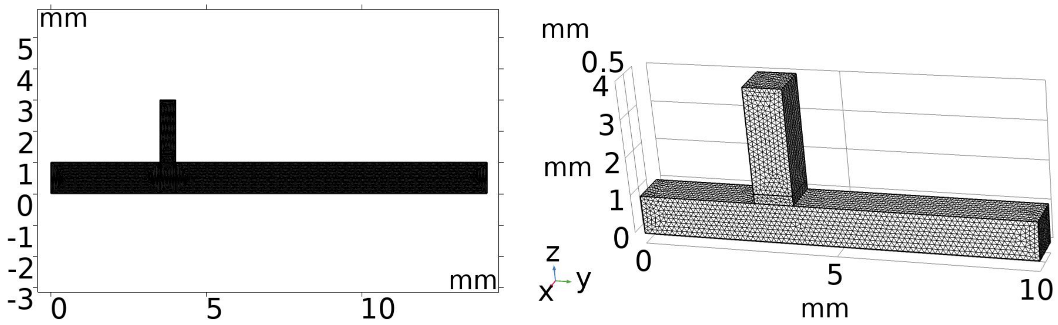

(A) (B)

Figure 2.1: COMSOL Multiphysics geometries for droplet generation. (A) 2D-geometry with mesh setting "finer". (B) 3D-geometry with mesh setting "coarse".

The physics interface applied were two-phase flow, laminar flow, level set. This is a multi physics interface, which combine laminar flow physics with the mathematical level set interface. The two-phase laminar flow module is applicable to two immiscible, the incompressible Navier-Stokes equations are solved:

$$\rho \frac{\partial \mathbf{u}}{\partial t} + \rho \left(\mathbf{u} \cdot \nabla \right) \mathbf{u} = \nabla \cdot \left[-p\mathbf{I} + \mu \left(\nabla \mathbf{u} + \nabla \mathbf{u}^T \right) \right] + \mathbf{F_g} + \mathbf{F_{st}}$$

$$\nabla \cdot \mathbf{u} = 0,$$

where ρ is the density, $\mathbf{u}$ is the velocity field, p is the fluidic pressure, $\mathbf{I}$ is the unit diagonal matrix, μ is the dynamic viscosity, $\mathbf{F_{st}}$ is the surface tension force acting on the interface between the two fluids, and $\mathbf{F_g}$ is the gravity force.

The level set interface, is a way to represent the two phases. By defining ϕ, the level set function, which is 0 in one phase and 1 in another a representation of two phases are made. There are some parameters to set in order for the level set function to work properly, these are interface thickness parameter ϵ, which determines the thickness of the domain where ϕ goes from 0 to 1. The reinitialisation parameter γ, which should be around the maximal magnitude of the velocity field. Furthermore the contact angle, surface tension coefficient and slip length are to be defined, these are important for the laminar flow calculations. For the simulations ϵ were $1 * 10^{-4}$, γ were 0.1 m/s, the contact angle were 135°, the surface tension coefficient were 0.1 N/m and, the slip length were $5 * 10^{-5}$. The continuous phase $\phi = 1$ properties were set as for a 20% PVP in 4:1$EtOH$ solution. The density were 1 g/mL and the viscosity were measured to be 335 cp by a Viscolite 700 viscometer. The dispersed phase ϕ=0 properties were set as for GSO. The density were 0.921 g/mL and the viscosity were measured to be 55 cp. The droplet diameter were evaluated automatically by the formula:

$$d = 2 \cdot \sqrt{\frac{\int_y \int_{x=9.5}^{x=\infty} dA}{\pi}} \quad \text{for}\, \phi < 0.5 \,\text{and}\, x > 9.5\text{mm}.$$

for 2D simulation or the formula:

$$d = 2 \cdot \sqrt[3]{\frac{\int_z \int_x \int_{y=7}^{y=\infty} dV \cdot 4}{3 \cdot \pi}} \quad \text{for}\, \phi < 0.5 \,\text{and}\, y > 7\text{mm}.$$

for 3D simulation.

2.5 Emulsion Electrospinning

Emulsion electrospinning were done with the same setup as for conventional electrospinning, but the spinneret consisted of a 3D-printed droplet generator where the crocodile clamp was attached directly to the outlet. This facilitated generation of the Taylor cone directly from the droplet generator. For droplet generators with two dispersed phase inlets the Harvard Programmable PHD 2000 pump could support two syringes at once, however with identical flow rate. Tert-butylbenzoquinone (Sigma Aldrich, Lot# MKBS3733V) were added at a concentration of 100 mM to GSO.

2.6 Post-Electrospinning Treatment

After electrospinning the PVP fibres were unstable in water. In order to increase the water stability, the fibres, both mats and samples on glass plates, were treated in a Bioforce UV Ozonecleaner for 30 minutes. For mats both sides were treated for 30 minutes. This UV-curing approach was inspired by Faria et. al [60].

2.7 Fluorescence Measurements

Fluorescence measurements were performed with an ISS chronos DFD fluorescence lifetime spectrometer (model 90021, serial 1067). TBBQ were excited at 285 nm and emission were measured between 295 and 360 nm. For the calibration curve a set of aqueous TBBQ solutions were made and measured, a linear fit through zero were used to determine the slope. For the release measurements, a weighed amount of sample was put in a 5 mL eppendorf tube, then 4 mL deionised water were added. Between each time the tube was shaken, 400 µL were added to a quartz cuvette and measured, the volume was then added to the tube again.

CHAPTER 3

RESULTS

3.1 Fabrication of 3D-Printed Microfluidic Droplet Generators

Initial testing of 3D-printing settings, did produce a set of optimal printing parameters. Channel sizes of 500 µm were obtainen. However, a minimum channel size of 600 µm were established, in order to obtain a success rate above 25% when 3D printing.

After initial testing of settings, different droplet generator schematics were made. In total 186 different CAD files were tested, however, many where different sizes of the same design. There were flow-focusing, co-flow, and cross-flow junctions, only a single schematic were made for the co-flow junction (fig. 3.1a). In this design a tube inside the main channel supplied the dispersed phase. However, the 3D-printing were unsuccessful, as the channel clogged at the droplet generation site. Various flow-focusing junctions were tested, the droplet generation site principle were kept constant, but the sizes were varied (fig. 3.1b). Further progress with the flow-focusing geometry were halted, as reliable printing of an inlet with 2 sub-channels proved difficult.

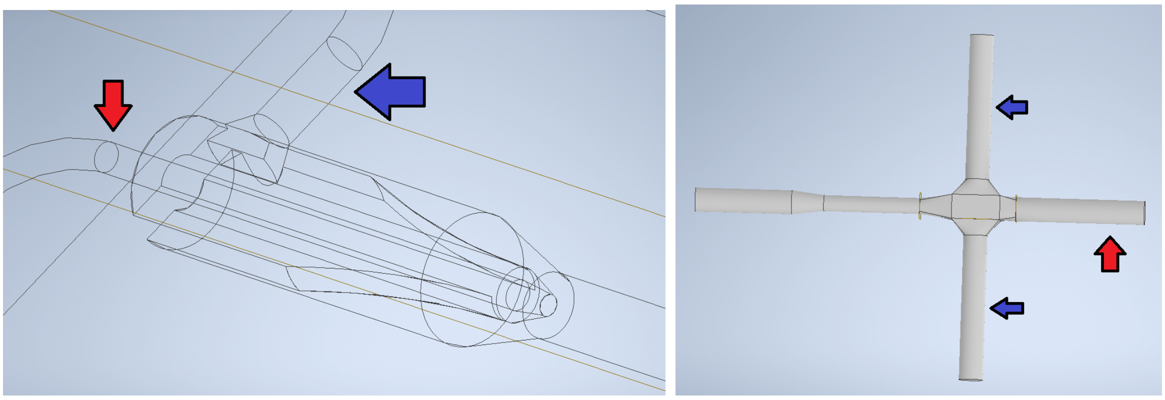

(A)

(B)

FIGURE 3.1: Schematic of droplet generator designs (A) The co-flow droplet generator (B) Flow-focusing droplet generator. The blue arrows indicate inflow of continuous phase, the red arrows indicate inflow of dispersed phase.

The T-junction had the largest focus, due to its simple geometry several different T-junction designs were tested. First a simple T-junction (fig. 3.2a) were made for various sizes, with both heterogeneous and homogeneous channel diameters. Secondly, the principle of multiple T-junctions on the same channel were tested (fig. 3.2b) in order to increase the frequency of droplets. Variations with up to 20 junctions in one were tested. However, no successful prints were obtained, as all the channels never were open at the same time.

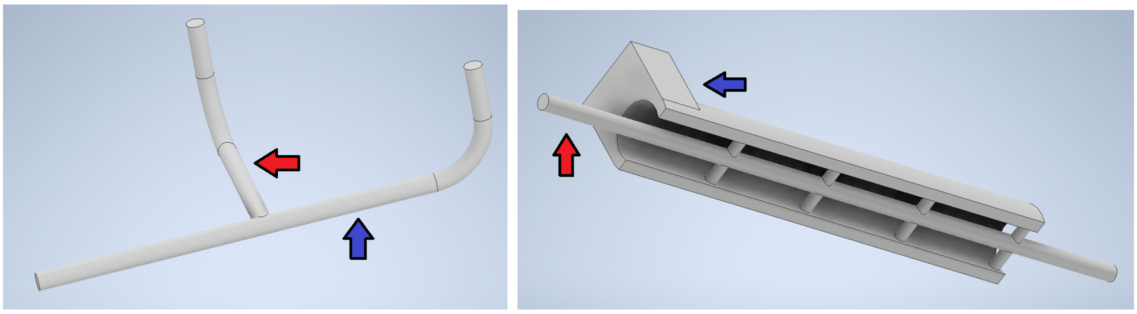

(A)

(B)

Figure 3.2: Schematic of droplet generator designs. (A) The simple T-junction generator (B) The multiple T-junction droplet generator. The blue arrows indicate inflow of continuous phase, the red arrows indicate inflow of dispersed phase.

After the realisation of multiple junctions in one channel were unfeasible, a design of a T-junction with at variable channel height were tested. This design should enable precise control of size and frequency of the produced droplets. The design (fig. 3.3a) is a simple T-junction with at screw-nut system above, where the nut contain a piston located above the droplet generation site. The system worked to some extent, however reliable reproduction of results were difficult, as each individual measurement were with a different channel height. Finally, a T-junction design where two T-junctions each with at separate channel were designed (fig. 3.3b), the problem with one inlet to two channels were overcome by introducing a rectangular chamber, which eased the cleaning of the channels. The two channels flow together just before the outlet, thus preventing coalescence of the droplets prior to electrospinning.

The design with two dual T-junctions were fabricated with different channel sizes, however final diameters were 1mm for the continuous phase channel and 0.75mm for the dispersed phase channels. This specific droplet generator were used for the final emulsion electrospinning experiments.

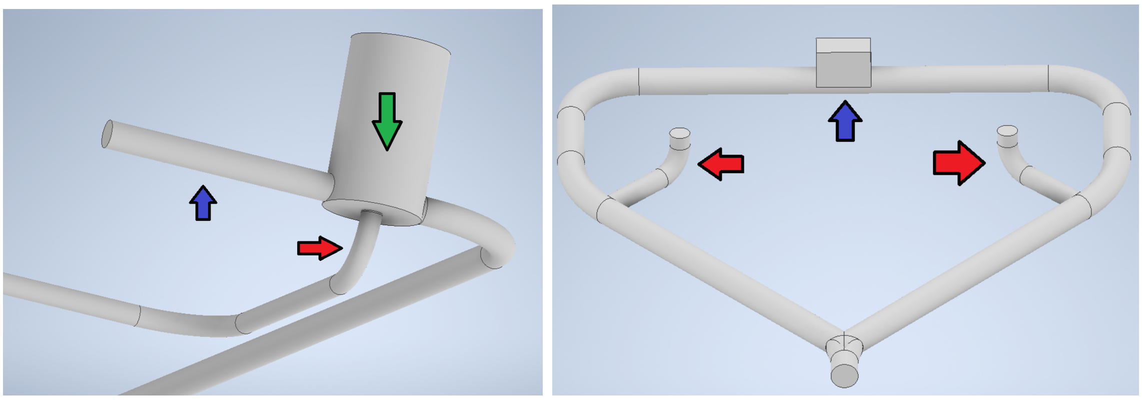
(A) (B)

FIGURE 3.3: Schematic of droplet generator designs. (A) The screw-nut droplet generator (B) The dual channel droplet generator. The blue arrows indicate inflow of continuous phase, the red arrows indicate inflow of dispersed phase, and the green arrow indicate the direction of the screw piston.

3.2 Droplet Generation with 3D-printed Droplet Generator

The generation of droplets were tested prior to emulsion electrospinning. There were used two different set of flow rates for the final emulsion electrospinning. For the first set, the continuous phase where set to 80µL/min and the two dispersed phases were set to 16.5 µL/min each. For the second set the continuous phase where set to 50µL/min and the two dispersed phases were set to 12.5µL/min each (table 3.1).

TABLE 3.1: The two flow rate sets used for droplet generation in the dual droplet generator.

Flow rate set	Contiunous phase flow rate [µL/min]	Dispersed phase flow rate [µL/min]
1	80	16.5
2	50	12.5

The diameter of the produced droplets (fig. 3.4), when the continuous phase were 20% PVP and the dispersed phase were GSO, can be seen in (table 3.2). It seems like flow rate set 1 produces satellite droplets, significantly smaller than the other droplets generated (fig. 3.4a). The same tendency can not be seen for droplet generation with flow rate set 2 (fig. 3.4b). The droplets were generated approximately at a frequency of 1 droplet per 2 second per inlet for both flow rate set 1 and 2.

Table 3.2: Table of measured droplet diameters, for two different flow rate sets, with 20% PVP in 4:1 $EtOH : H_2O$ as continuous phase and GSO as dispersed phase.

Flow rate set	Droplet diameter [mm]	Standard deviation [mm]
1	0.469	0.213
2	0.742	0.0159

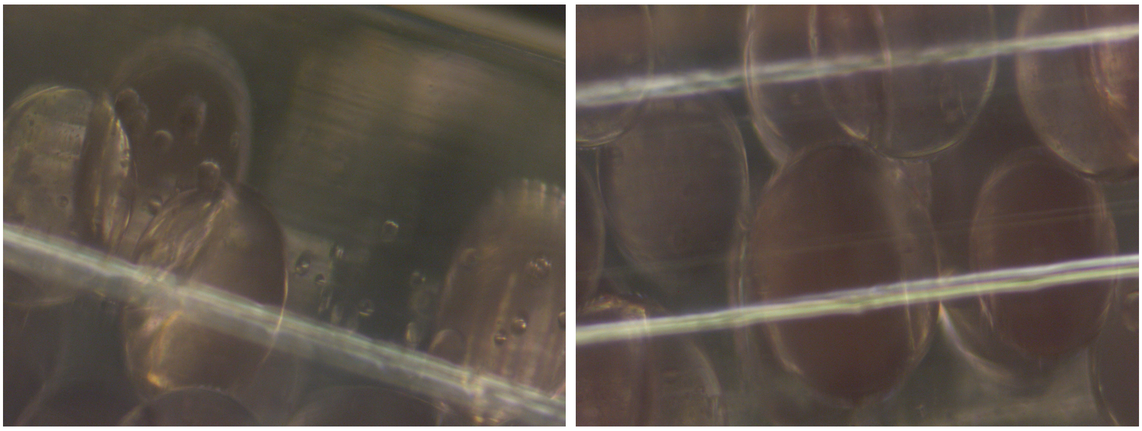

(A) (B)

Figure 3.4: Images of droplets produced the 3D-printed dual droplet generator, with 20% PVP in 1:4 $EtOH : H_2O$ as continuous phase and GSO as dispersed phase. The flow rates were (A) 80 and 16.5 µL/min (B) 50 and 12.5 µL/min for continuous flow and dispersed flow, respectively.

3.2.1 2D and 3D COMSOL Multiphysics Simulation of Droplet Generation

COMSOL Multiphysics simulation of the droplet generation were simulated in both 2D and 3D. With geometry matching the dual droplet generator simulations were performed for different time intervals. 2D simulations were simulated for 15 seconds and 3D simulations were simulated for 50 seconds. The diameters calculated are within a reasonable range from each other (table 3.3). However, the droplets have diameters larger than the channel they were within (1000 µm), from figs. 3.5 and 3.6 this is also evident, as the droplets are elongated into elliptical shapes. There is more than a two times difference between the measured diameter of the produced droplets and the simulated droplets c.f tables 3.2 and 3.3. Furthermore, there are no satellite droplets produced for flow rate set 1 in the simulations c.f figs. 3.4a, 3.5a and 3.6a. The simulated droplets were generated approximately at a frequency of 1 droplet per 5 seconds for both flow rate set 1 and 2.

TABLE 3.3: Droplet diameters of droplets simulated in COMSOL Multiphysics for two different flow rate sets.

Flow rate set	2D Simulation [µm]	3D Simulation [µm]
1	1421.6	1526.5
2	1430.2	1568.3

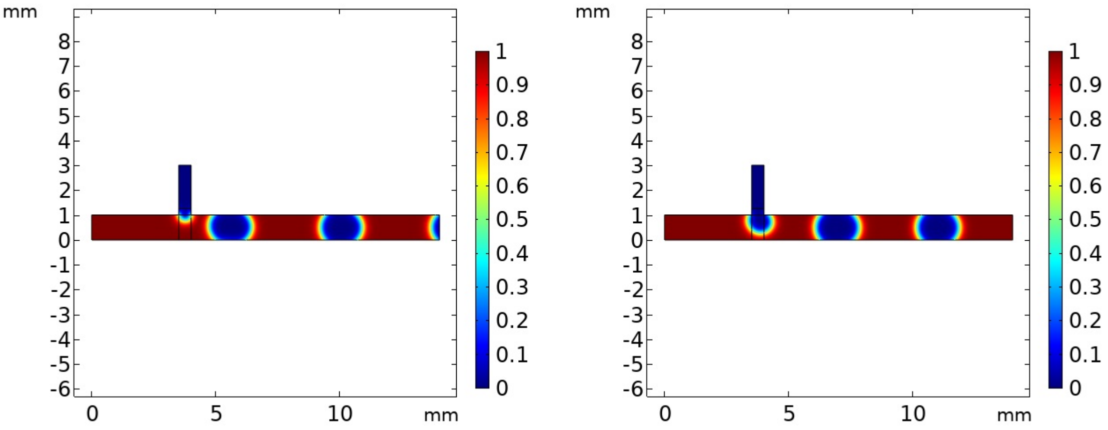

(A) (B)

FIGURE 3.5: 2D COMSOL Multiphysics simulations of droplet generation by the dual droplet generator. The scale bar indicates the level set function, i.e. 1 for continuous phase and 0 for dispersed phase. The dispersed phase flow rate set were (A) 1 (B) 2.

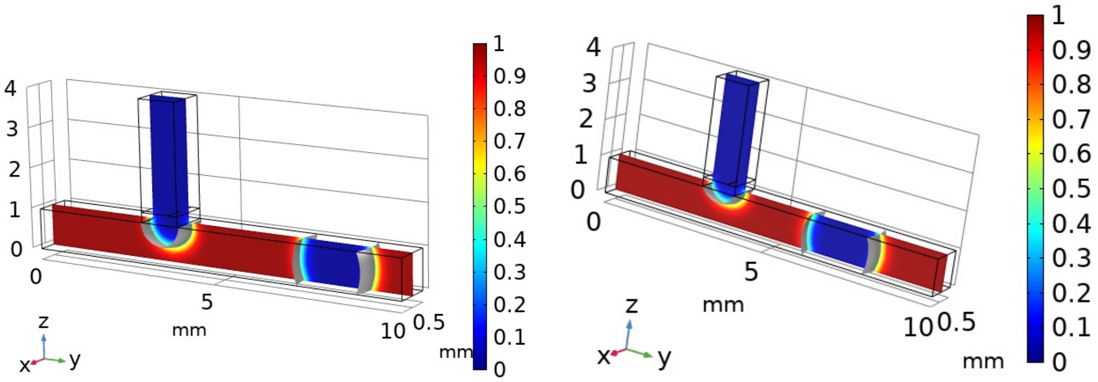

(A) (B)

FIGURE 3.6: 3D COMSOL Multiphysics simulations of droplet generation by the dual droplet generator. The scale bar indicates the level set function, i.e. 1 for continuous phase and 0 for dispersed phase. The dispersed phase flow rate set were (A) 1 (B) 2.

3.3 Conventional Electrospinning of Polymers

Prior to emulsion electrospinning, the polymers ability to be electrospun were tested by conventional electrospinning. In (table 3.4) a list of the different polymer solution which were tested can be seen. Each solution were tested for conventional electrospinning, however, if it were able to be electrospun conventionally, emulsion electrospinning were tested. For those where emulsion electrospinning is denoted as not possible, even though conventional electrospinning were possible, problems regarding the spinning process occurred during emulsion electrospinning. All emulsions with hydrophilic polymer solutions were with GSO as the dispersed phase, however, for the hydrophobic polymer solutions either glycerol or deionised water was the dispersed phase.

TABLE 3.4: A list of the different polymers tested, the solvent used, whether or not it was able to be electrospun either as conventional or emulsion electrospinning, the collector-distance, and the voltage applied.

Polymer [w/V Concentration]	Solvent	Electrospinnable	Electrospinnable Emulsion	Distance cm	Voltage kV
Carboxymethyl cellulose Mw=250kDa [4%]	H_2O	No	No	N/A	N/A
Polyethylene oxide Mw=300kDa [8%]	H_2O	Yes	No	9	12
Polyethylene oxide Mw=5000kDa [2%]	H_2O	No	No	N/A	N/A
Starch [5%]	H_2O	No	No	N/A	N/A
Polyvinylpyrrolidone Mw=360kDa [15%]	H_2O	No	No	N/A	N/A
Polyvinylalcohol Mw=89-98kDa [10%]	H_2O	Yes but beaded	No	9	17
Polyvinylalcohol Mw=89-98kDa [7.5%] Polyvinylalcohol Mw=72kDa [7.5%]	H_2O	Yes	No	15	16
Polyvinylpyrrolidone Mw=360kDa [10%] Polyvinylalcohol Mw=72kDa [10%]	H_2O	Yes	No	21	21
Polycaprolactone Mw=80kDa [10%]	Chloroform	Yes	No	21	22
Polyvinylidene fluoride Mw=275kDa [6.5%]	2:1 Acetone:DMSO	No	No	N/A	N/A
Polyvinylidene fluoride Mw=275kDa [10%]	2:1 Acetone:DMSO	No	No	N/A	N/A
Polyvinylidene fluoride Mw=275kDa [16%]	2:1 Acetone:DMSO	Yes	No	21	12
Cellulose acetate Mw=30kDa [12.5%]	Acetone	Yes	No	9	16
Polycaprolactone Mw=80kDa [15%]	Acetone	Yes	No	21	18
Polyvinylpyrrolidone Mw=360kDa [20%]	Ethanol	Yes but beaded	No	21	23
Polyvinylpyrrolidone Mw=360kDa [20%]	4:1 Ethanol:H_2O	Yes	Yes	21	2
Gelatine [10%]	Trifluoroethanol	Yes	No	1	1
Gelatine [30%]	30% Acetic acid	Yes	No	1	1
Cellulose acetate Mw=30kDa [20%]	80% Acetic acid	Yes but beaded	No	N/A	N/A
Polycaprolactone Mw=80kDa [14%]	Trifluoroethanol:H_2O 5:1	Yes	No	21	22

3.4 Emulsion Electrospinning

Initial testing of emulsion electrospinning revealed that droplets should be produced with at specific size and frequency of generation. Therefore, several different combinations of flow rates were tested, for the system with a 20% PVP in 1:4 $EtOH : H_2O$ solution as the continuous phase and GSO as the dispersed phase. In order to establish how the emulsions are arranged inside the electrospun fibres, testing were performed with the fluorophore Nile Red in GSO. This allowed to see which part of the fibre the oil was located in. Distinct separation between the individual spindle-like droplets can be seen indicating closed compartments of GSO within the fibre (fig. 3.7).

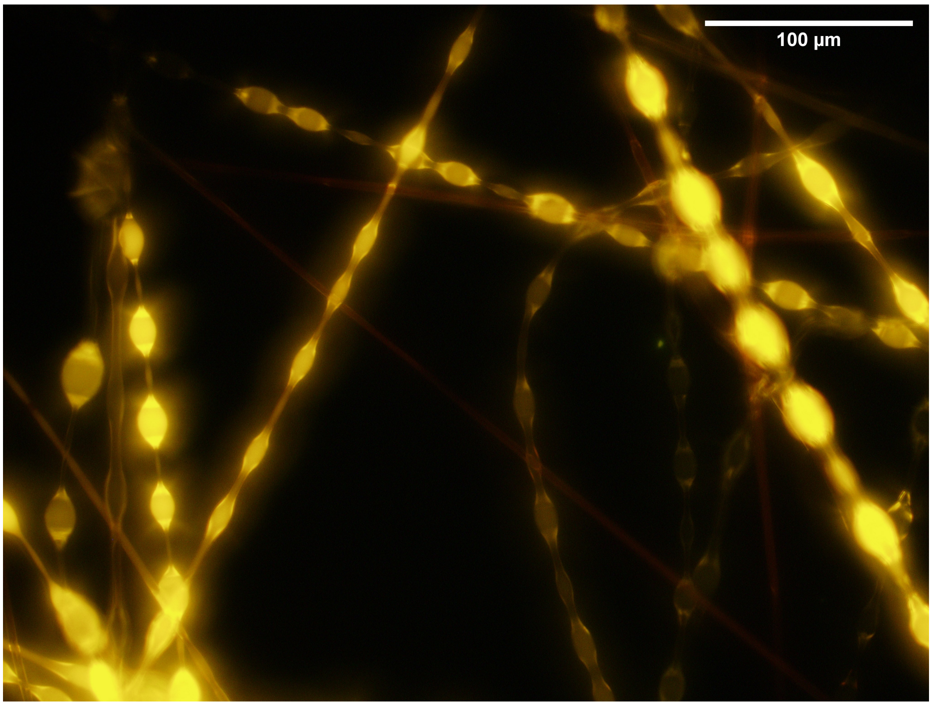

FIGURE 3.7: Fluorescence image of emulsion electrospun PVP fibres with Nile Red in the dispersed phase GSO. The fibres are illuminated with a FITC filter exciting the fluorophore. The fibres were electrospun at 21kV with 21cm distance, RH = 33% and the magnification are x40. The scale bar is 100 µm.

The final electrospinning were done with the flow rate sets described in (section 3.2). The samples produced with flow rate set 1 were denoted sample 210428, whereas the samples produced with flow rate set 2 were denoted sample 210510. Sample 210428 were spun at a relative humidity of 30%, whereas sample 210510 were spun at a relative humidity of 65%. Both samples were spun at 21 kV.

When imaging with SEM, some collapsed compartments were visible as "wet" areas, which looked like the fibre mat were wet (fig. 3.8). There are a significant difference in the amount of compartments visible in sample 210510 and 210428 c.f (figs. 3.8 and 3.11)

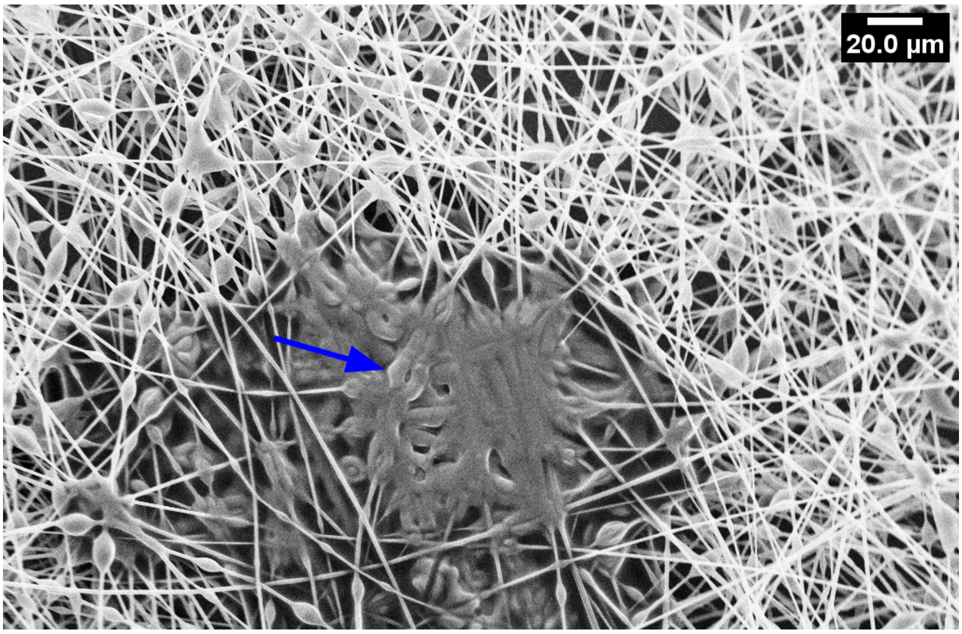

Figure 3.8: SEM image of sample 210510. The continuous phase were 20% PVP, at 50 µL/min, the dispersed phase were 100mM TBBQ, at 2x12.5 µL/min in the dual droplet generator. The blue arrow indicate a possible collapsed compartment. The scale bar is 20 µm. The fibres were electrospun at 21kV with 21cm distance and RH = 65%.

It was of interest to examine the effect of water on the UV-cured electrospun fibres, as uncured fibres were water soluble. The UV-curing seems to induce collapse of compartments in the lower layers of fibres (fig. 3.9). The same smeared lower layering is not seen for uncured fibres (fig. 3.12). Furthermore is it evident that water does have some effect on the fibres after UV-curing, the fibres appear partially dissolved and are cracked (fig. 3.10).

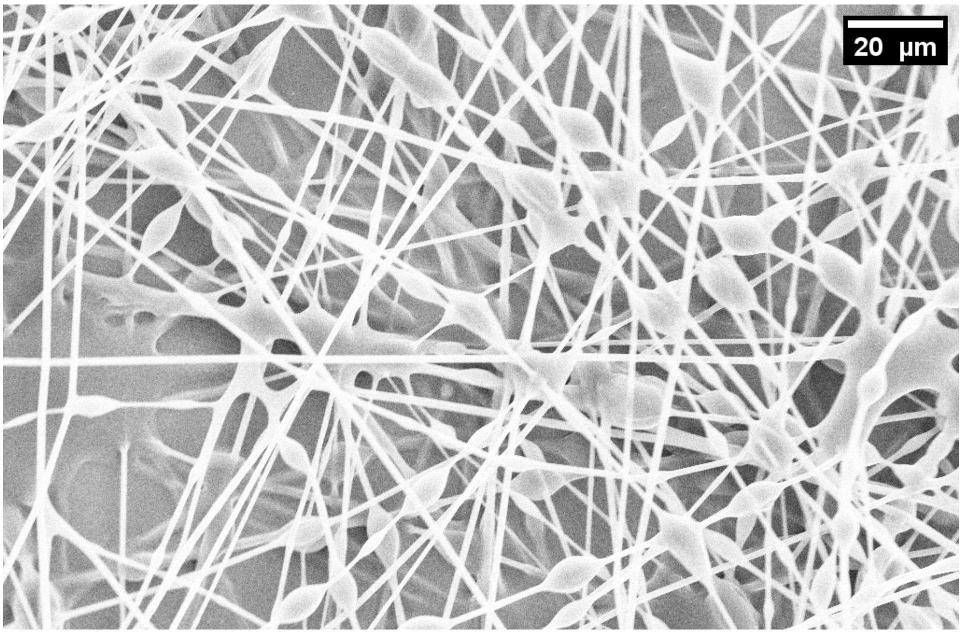

Figure 3.9: SEM image of sample 210510 after UV-curing. The continuous phase were 20% PVP, at 50 µL/min, the dispersed phase were 100mM TBBQ, at 2x12.5 µL/min in the dual droplet generator. The scale bar is 20 µm. The fibres were electrospun at 21kV with 21cm distance and RH = 65%.

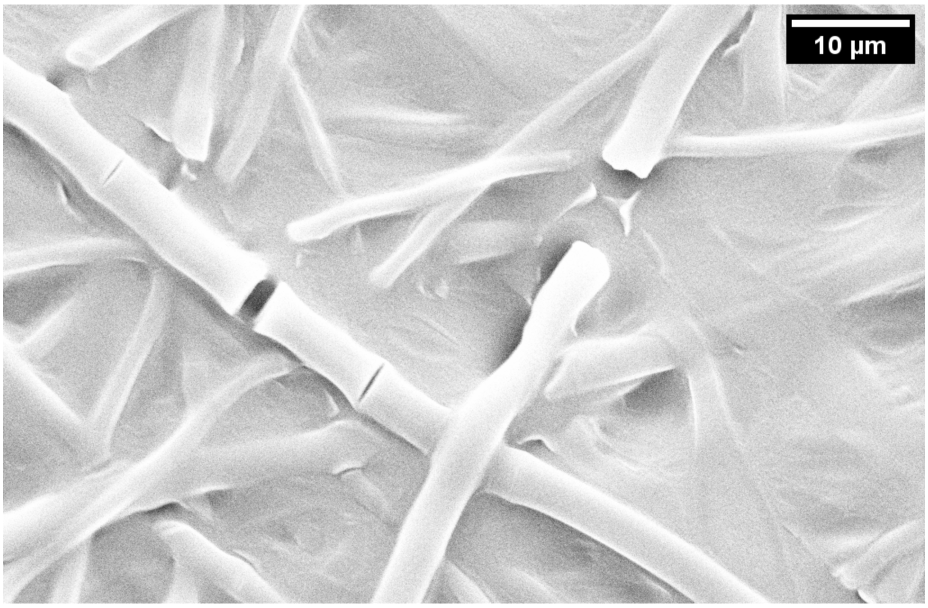

Figure 3.10: SEM image of sample 210428, after being submerged in deionised water. The continuous phase were 20% PVP, at 80 µL/min, the dispersed phase were 100mM TBBQ, at 2x16.5 µL/min in the dual droplet generator. The scale bar is 10 µm. The fibres were electrospun at 21kV with 21cm distance and RH = 30%.

Another interesting part of the fibres are the diameter of the compartments. Two compartments and their corresponding fibre were measured for both sample 210510 and 210428. The specific compartments measured are marked either 1 or 2 (figs. 3.11

and 3.12). The measured diameters can be seen in table 3.5. The two compartments measured for sample 210428 were 6.564 and 6.432 µm in diameter with standard deviations of 0.181 and 0.136 µm. The corresponding fibre diameter were between 2.486 and 2.022 µm, with standard deviations of 0.103 and 0.108 µm. These two compartments were located on the same continuous fibre, as only one fibre with compartments were visible.

The two compartments measured for sample 210510, were on two different fibres and were 3.529 and 2.855 µm in diameter, with standard deviations of 0.078 and 0.135 µm. The corresponding fibre diameters were 1.178 and 0.897 µm, with standard deviations of 0.041 and 0.061 µm.

TABLE 3.5: Diameter of compartments and fibres for sample 210510 and 210428, measured from SEM images.

Sample	Diameter [µm]	Std. Deviation [µm]
210428-Fibre 1	2.486	0.103
210428-Compartment 1	6.564	0.181
210428-Fibre 2	2.022	0.108
210428-Compartment 2	6.432	0.136
210510-Fibre 1	1.178	0.041
210510-Compartment 1	3.529	0.078
210510-Fibre 2	0.897	0.061
210510-Compartment 2	2.855	0.135

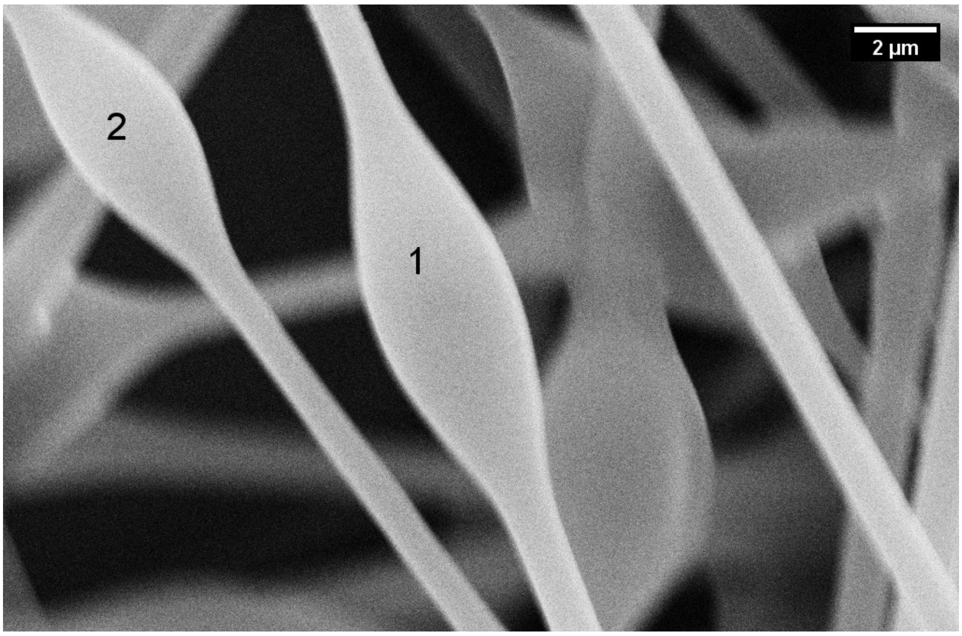

Figure 3.12: SEM image of sample 210510. Fibres 1 and 2 are tagged with numbers. The continuous phase were 20% PVP, at 50 µL/min, the dispersed phase were 100mM TBBQ, at 2x12.5 µL/min in the dual droplet generator. The scale bar is 2 µm. The fibres were electrospun at 21kV with 21cm distance and RH = 65%.

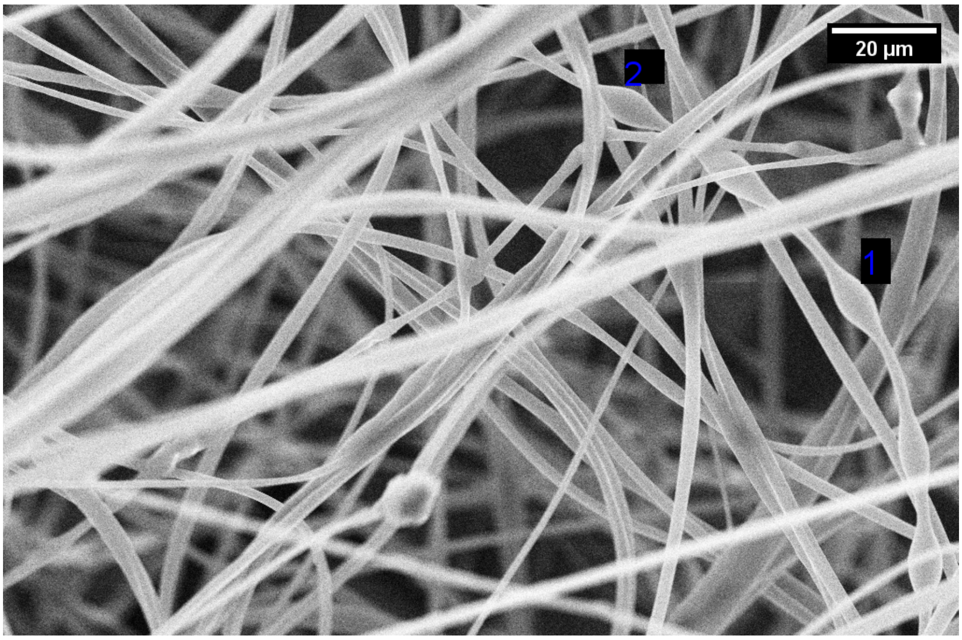

Figure 3.11: SEM image of sample 210428. Fibres 1 and 2 are tagged with numbers. The continuous phase were 20% PVP, at 80 µL/min, the dispersed phase were 100mM TBBQ, at 2x16.5 µL/min in the dual droplet generator. The scale bar is 20 µm. The fibres were electrospun at 21kV with 21cm distance and RH = 30%.

The release of TBBQ from UV-cured sample 210428 and 210510 into water were tested by fluorescence signal. A calibration curve were established in order to convert intensity to concentration. The calibration curve were fitted with a linear regression plot revealing a slope of 29500 fluorescence intensity unit/mM, with a regression coefficient of 0.96543 (fig. 3.13).

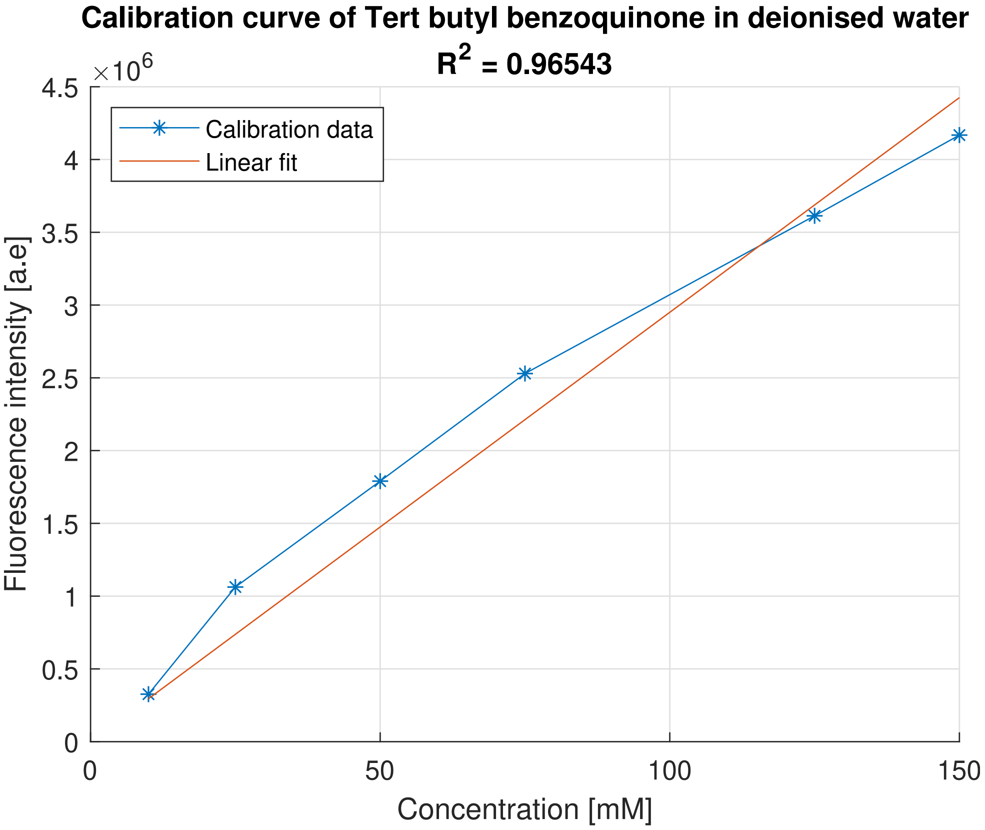

FIGURE 3.13: Calibration curve for TBBQ in deionised water. Excitation were at 285 nm and emission at 330 nm.

Fluorescence measurements were taken for different time intervals, and the intensity were converted to the cumulative release in percent. For both samples similar release profiles are seen (figs. 3.14 and 3.15), a fast increase up until a constant percentage. For sample 210510 smaller time intervals reveal that the increase happens rapidly within the first few minutes, already stabilising at around 17% after 3 minutes. However, for sample 210428 around 35 minutes are required for a constant around 10%. Furthermore, for sample 210428 an experiment where the initial 4 mL of water was replaced by 4 mL of fresh deionised water in order to establish if all TBBQ was released. It is seen that a similar tendency is seen, however the curve flatten at 3% instead of 10%. It is also seen that the standard deviation on the fluorescence measurement is small compared to the measured value, as standard deviation were in the range of 1000 [a.u.] compared to <250000 [a.u] for the measured values.

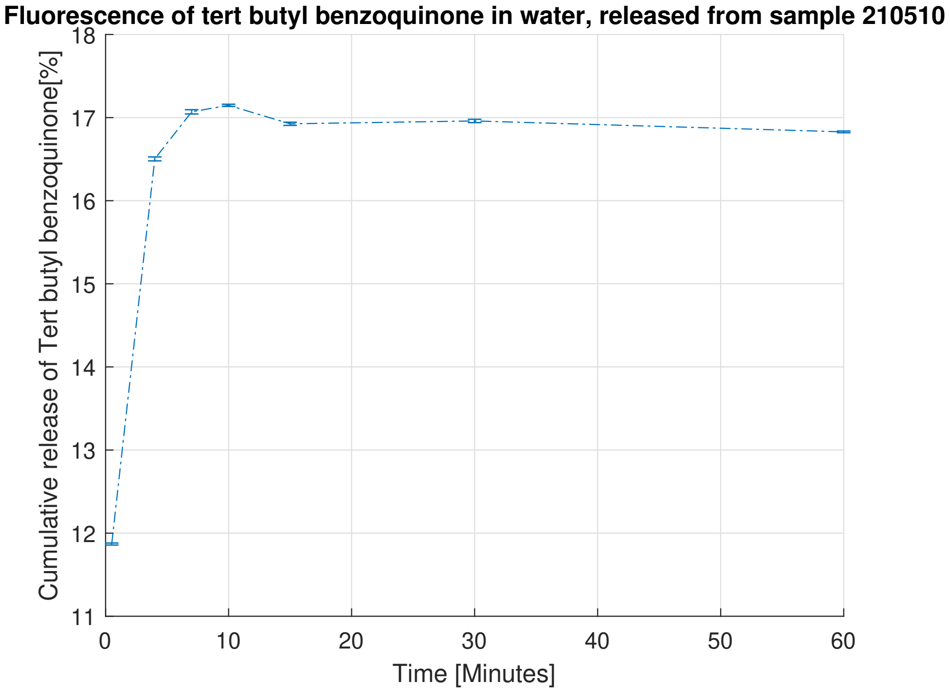

Figure 3.14: Release profile of TBBQ from electrospun sample 210510 into deionised water. Excitaion were at 285 nm and emission at 330 nm. The error bar indicate the standard deviation of each individual data point.

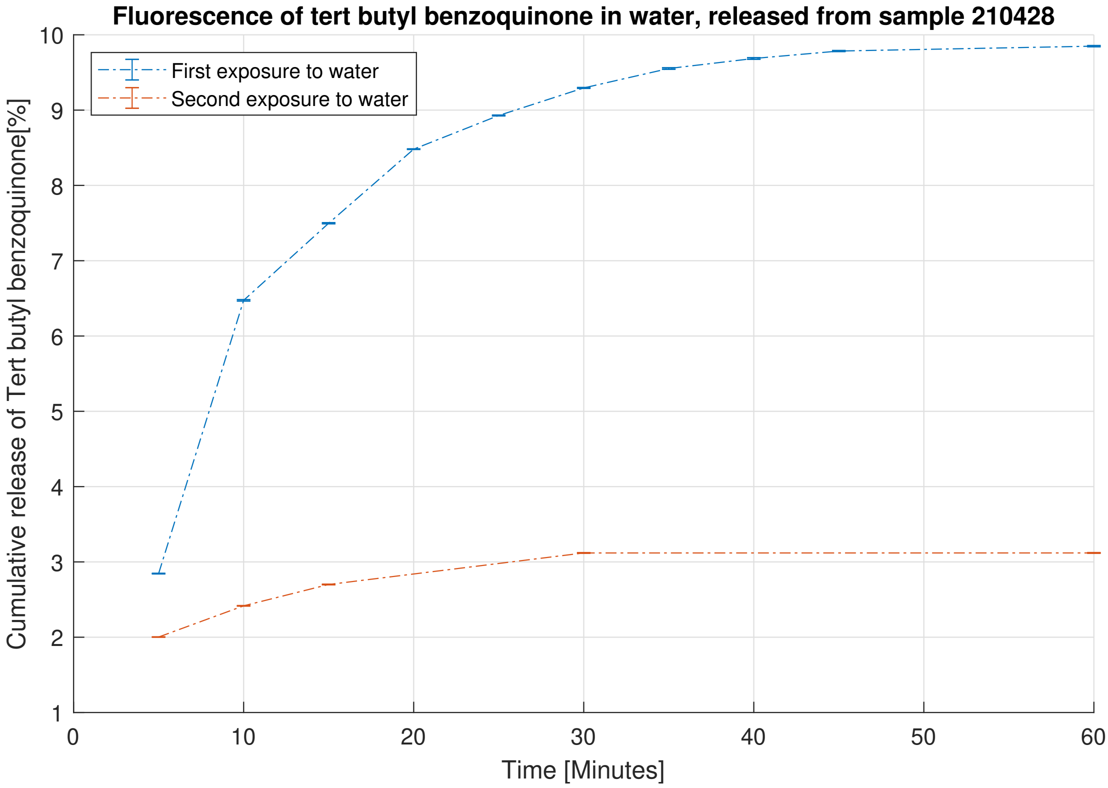

Figure 3.15: Release profile of TBBQ from electrospun sample 210428 into deionised water. Excitaion were at 285 nm and emission at 330 nm. The error bar indicate the standard deviation of each individual data point.

Chapter 4

Discussion

Encapsulation of TBBQ in Emulsion Electrospun Fibres

The purpose of emulsion electrospinning was to prevent burst release of the encapsulated compound, that are experienced in some core-shell fibres. There are different release patterns, zeroth order release is a constant release independent on the concentration at a given time. The zero order release are ideal for drug delivery systems, as these prevent burst release, however, if the release constant is large, quick depletion, and thus burst like release might be seen. Such zero order tendencies can not be seen for either sample 210510 or 210428 (figs. 3.14 and 3.15). There is also the possibility of first order release. For first order release the concentration of TBBQ at a given time will influence the release rate i.e a release rate decreasing over time. In order to establish if a release profile follows first order release, plotting the logarithm of amount of TBBQ not released over time. If this plot is linear it is a first order release.

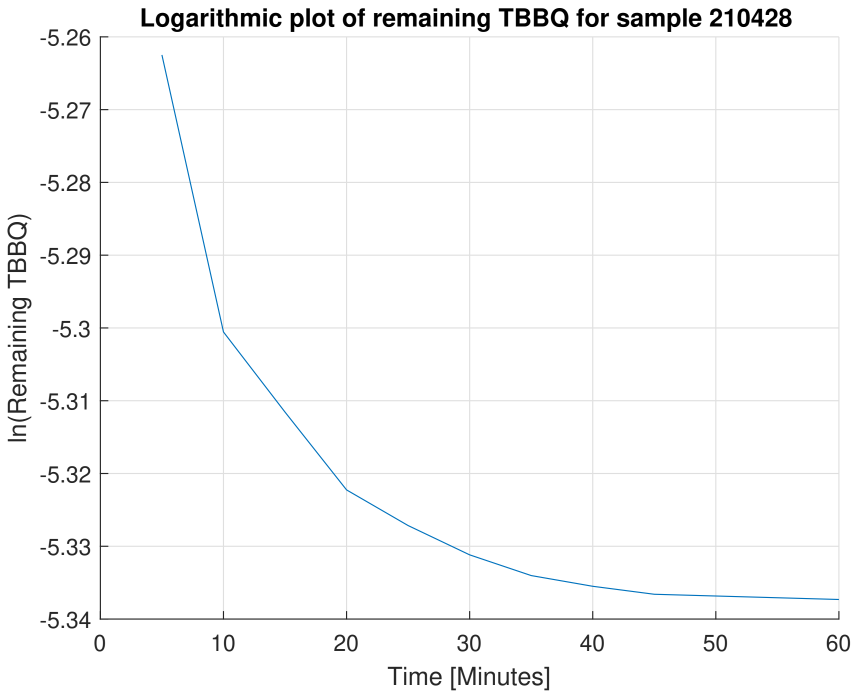

Figure 4.1: Logarithmic plot of remaining TBBQ in sample 210428. The nonlinear tendency indicate that the profile is not first order.

By observing (figs. 3.14 and 3.15) a gradually decreasing release is seen for sample 210428. However, when plotting the logarithmic of remaining TBBQ over time (fig. 4.1) no linear tendency is observed, which indicate that the release does not follow first order kinetics. [61]

It is worth noting that the initial release for sample 210510 is very rapid, where a maximum is reached after 7 minutes. Though only data points at 1, 4 and 7 minutes are available, the first section could be a very quick constant release. However, it is not possible to prove. By observing the data from the second release from sample 210428 (fig. 3.15) it is possible that the release is a simple equilibrium between TBBQ in GSO and water. The structure of TBBQ is hydrophobic, which could indicate that only a portion of TBBQ is able to get into the water. This would also explain why the maximum released for the second exposure to water were lower than the first, as the concentration of TBBQ in the encapsulated GSO were lower. The fact that release is determined by equilibrium might be beneficial for drug delivery systems. If the concentration of TBBQ is adjusted to an optimum, the fibres might sustain a concentration above the minimal therapeutic concentration. The concentration would however decrease as TBBQ is depleted. The maximum % TBBQ released for sample 210510 and 210428 were quite different, 17 and 10%, respectively. This might be due to the TBBQ/GSO solution, the sample were freshly prepared for sample 210428, whereas the solution were 2 weeks old when sample 210510 were produced. Some inhomogeneities in the solution could introduce concentration differences, which are not taken into account when calculating the cumulative release of TBBQ.

The nick observed on fig. 3.14 at the peak are difficult to explain, the error bar are too small for it to be insignificant. However, it might be an indication that multiple measurements should be done of each sample. The release profiles for sample 210510 and 210428 are not typically seen, as initial burst release often will be followed by a slower subsequent release. This tendency were seen by Nasari et. al when producing PCL/PVP core-shell fibres loaded with carbon nanotubes (fig. 4.2) [62]. [44], [46]–[48], [61]–[63]

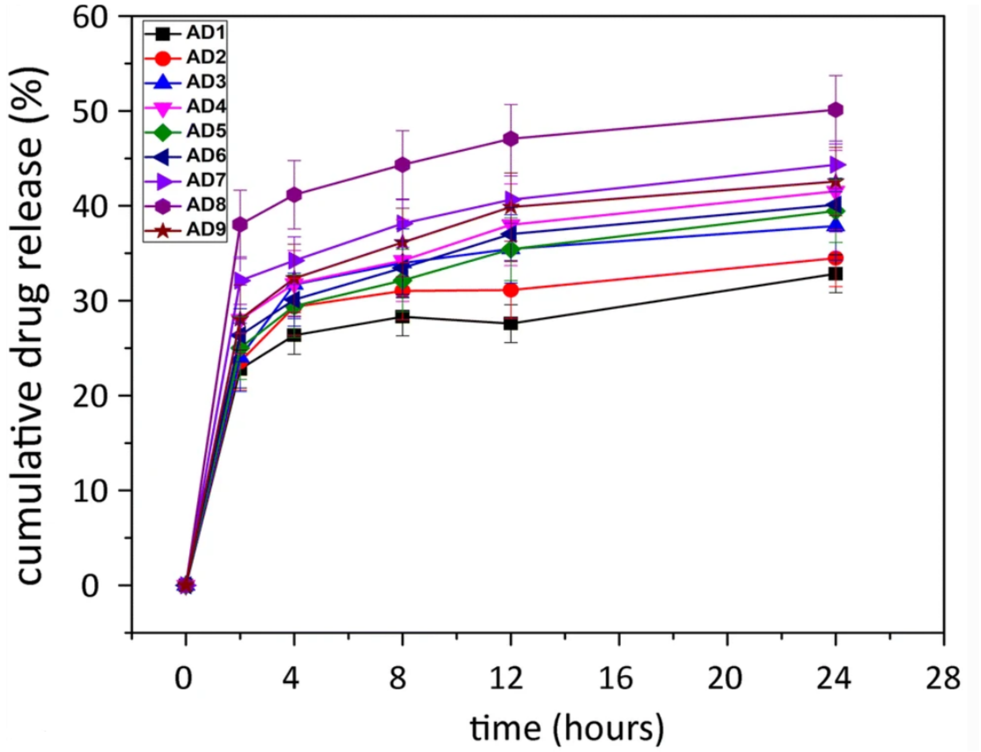

FIGURE 4.2: Cumulative release of 5FU from various nanofibers mat. Reprinted by permission from [Springer Nature]. [62]

From the release profiles it is clear that water were in contact with the encapsulated GSO. If this contact were due to collapse of the compartments, as seen for dried fibres (fig. 3.8) or if it is contact through the PVP shell are unknown. The release profiles might also be dependent on the amount of shaking, as it were by hand and with no specific procedure. The UV-curing of the fibres did seem to only cross-link the outer layer of fibres, as the background on fig. 3.9 seem to be collapsed fibres. This collapse of fibres should also be visible in the release profiles as the barrier between GSO and water is broken. However, the release profile for sample 210428 had no extremely rapid release, however, the equilibrium were reached after 30 minutes. It might indicate that PVP are not the best suited polymer for this release system. Several other both hydrophillic and hydrophobic polymers were tested, though some could be electrospun, the emulsion electrospinning were impossible, this might be because of the difference in emulsion characteristics or the parameters at which the polymer could be electrospun. It was evident that the size of the droplets generated were crucial for the resulting fibre morphology. This is interesting, as the produced droplets had diameters of several 100 µm, while the compartments produced had diameters of only a few µm. This tendency could indicate a secondary droplet generation site within the Taylor cone, most likely due to a pseudo flow-focusing geometry at the tip of the Taylor cone. However, no experiments regarding this phenomena were conducted (fig. 4.3).

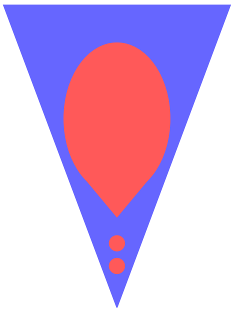

Figure 4.3: Schematic of the proposed secondary droplet generation site within the Taylor cone.

The parameters regarding electrospinning of the polymers were important, as a too low optimal flow rate would render a proper droplet generation frequency difficult to obtain. A too high optimal flow rate might prevent the secondary droplet generation, but rather force it into a continuous co-flow stream, thus resulting in core-shell fibres. It is evident that the frequency of fibres with compartments were highest for sample 210510, which had a lower total flow rate than sample 210428. However, in respect to release from the fibres sample 210428 did show the most sustained release profile. Whereas, sample 210510 had a faster release, this might be because of the increased surface area that arise from the compartments.
Furthermore, it was observed that a too low voltage would render emulsion electrospinning impossible, probably due to a lower charging of GSO. The pure PVP solution were able to be electrospun within a range of 11 to 30 kV, and tip-collector distances between 10-21 cm. For the PVP/GSO system, a minimal voltage for emulsion electrospinning were 20 kV, below this threshold it appeared as GSO were collecting at the tip of the droplet generator, as if only PVP were spun. Furthermore, the tip-collector distance were important, as electrospinning the PVP/GSO system at tip-collector distances below 18 cm did produce sputtering of GSO.

The hydrophobic polymers, were tested with water/glycerol as the dispersed phase. Some solvents, such as acetone, did prove difficult for emulsion electrospinning, due to solubility of acetone and water. Acetone did mix with water to an extent were the polymer precipitated within the channel. There might have been further advances withing hydrophobic polymers, by utilising the less green solvent, such as dimethylformamid or dichloromethane. Chloroform were tested, but the flow and emulsions were not suited for emulsion electrospinning within the dual emulsion droplet generator.

In general it should be noted that all results are produced with the dual emulsion droplet generator, with the same channel sizes for all polymers. This fixed channel size could easily be the reason why some polymers were better than others, as the emulsion will be different in smaller channel but with the same flow rates.

Droplet Generation

Droplet generation in the dual droplet generator were successful with the PVP/GSO system. The flow rate set 1, corresponding to sample 210428, did produce droplets of varying size with additional small satellite droplets. The average droplet diameter for flow rate set 1 were 0.469 µm with a standard deviation of 0.213 µm. However, flow rate set 2, corresponding to sample 210510, produced significantly more monodisperse droplets with average diameter of 0.742 µm with a standard deviation of 0.0159 µm. The most dominant difference is in the standard deviation, as droplets produced by flow rate set 2 had a standard deviation significantly lower than for droplets produced by flow rate set 1. This difference might be due to the measuring method, which were done by hand in ImageJ, this method may be faulty due to bias when placing the edge of the droplet. Furthermore, the droplets were contained in a tube of 4 mm internal diameter, this allowed clusters of droplets in different heights within the same image. This difference in height will also have had an influence on the measured droplets dependent on the focal plane of the microscope. However, no experiments determining the specific impact were performed.

Both 2D and 3D COMSOL Multiphysics simulations of droplet generation by the two flow rate sets were performed. The droplet diameters simulated by 2D simulations were 1421.6 and 1430.2 µm and the droplet diameters simulated by 3D were 1526.5 and 1568.3 µm, for flow rate set 1 and 2, respectively. The difference for the different flow rate set in each model are small with 8 and 42 µm for 2D and 3D, respectively. However, a difference above 100 µm are observed between 2D and 3D. This difference might be due to the inherent differences in the model geometries. In 2D it were not possible to include that the dispersed phase inlet were shorter than the continuous phase channel in the third dimension. This were possible to include in the 3D model, which might explain the increased diameters observed, as the droplet can fill an even larger channel than perceived in 2D. It is easily observed that the droplets are larger than the channel, and plug the channel before droplet generation. This plug action present a fault in the equation which the diameters are calculated from, as these assume perfect spherical/circular droplets. However, when comparing the simulated droplet diameters with the measured ones there is roughly a factor 2 difference between them. This is probably due to the input settings for the simulations. The interfacial tension set between the GSO and PVP phases were 0.7 [N/m], according to Gaonkar [64] the interfacial tension between vegetable oils and water are around 0.003 [N/m]. There is a significant difference in these interfacial tensions. It would probably have a distinct influence on the simulation if this value were used. However, it is important to keep in mind that a 20% PVP in Ethanol and water solution have properties different than water, and direct measurements of the interfacial tension between GSO and the PVP solution would be the better approach. The same applies to the contact angle applied in the simulations which also should have been measured in order to obtain more precise simulations. Furthermore, the frequency of droplet generation were different between simulations and microfluidic droplet generation. The increased diameter in simulations, would be expected as the droplet generation frequency are lower, thereby, will more dispersed phase accumulate in the droplet before it is released. Further improvements of the models could be applying an adaptive mesh, with ensures the finest mesh elements track along the interface between the two phases.

3D Printing of Microfluidic Droplet Generators

The 3D printing process were the determining factor regarding channel sizes. The different designs were tested for various channel sizes, and the minimal channel diameter achieved were 500 µm for both square and circular channels. Both square and circular channels have been 3D printed in sizes down to 200 µm by Song et. al [52]. Various factors influence the minimal channel size that can be achieved.

The resin used will have limitations regarding the achievable size. This is due to the solidification, if the UV light are scattered sufficiently by the resin, an area larger than the pixel will solidify. The possibility of adding pigments to the resin will decrease the amount of scattering, by absorbing more of the light [65]. However, this approach might not be suitable for 3D printed microfluidics as the transparency is crucial for the applicability of the device. Colouring with a weak pigment, which in turn create coloured but transparent devices might be beneficial. Furthermore, the resin will have a critical minimal energy required by each pixel prior to solidification. If we think of the three dimensional pixels, voxels, the degree of solidification of these are proportional to the greyscale value given in the slicing software. Often will this greyscale be either max or min, however, some software add anti aliasing where boundary voxels are assigned an intermediate greyscale value in order to smooth out the edge. A significant consideration to this approach should be that the degree of solidification will go exponential to the greyscale value above the critical minimal energy. However, if the proper greyscaling can increase the resolution of 3D printers. [66]

The solidification of these voxels are generally of importance when producing microfluidics. As the partial scattering of light will influence neighbouring voxels within the channel space partial solidification will occur. This might prevent proper cleaning of the channel, or simply deform the channel with smaller channel sizes or growths within the channel. [65]

The most simple method of decreasing the amount of scattering, is by minimising the required exposure for each voxel. This can be done by testing various resins or alternatively blending a custom resin with a higher amount of photo initiator [65].

It is evident that the channel size might not exactly the predetermined one, and as mentioned earlier the size of the channel will have a significant influence on the produced emulsion, the channels in the dual droplet generator were in the large end of the microfluidic scale. No experiments of the 3D printed channel sizes were conducted. Furthermore, no experiments examining differences in droplet generation between two individual dual droplet generators were conducted. This could have been important in order to establish whether or not the 3D printing produced homogeneous droplet generators, and if it had any influence on the emulsion generated.

CHAPTER 5

CONCLUSION

The aim of the project were to fabricate emulsion electrospun fibres, with TBBQ encapsulated in a GSO phase. The emulsions were to be generated by 3D printed microfluidic droplet generators.

Emulsion electrospun fibres were produced with two different flow rate sets. The first flow rate set had a continuous phase flow rate of 80 µL/min and a dispersed phase flow rate of 16.5 µL/min. The second flow rate set had a continuous phase flow rate of 50 µL/min and a dispersed phase flow rate of 12.5 µL/min. The continuous phase were a 20% PVP in 4:1$EtOH : H_2O$ solution. The dispersed phase were GSO with 100 mM TBBQ. The second flow rate set produced sample 210510 which had the highest frequency of compartments visible on the electrospun fibres. Sample 210428, which were produced by flow rate set 1, did show a few compartments. The release profiles for the two samples were quite different. Sample 210428 had a gradually decreasing release rate until equilibrium were met. Sample 210510 had a more rapid release until the equilibrium were met. Sample 210510 had a cumulative release of 17% compared to 10% for sample 210428. The compartments on the fibre were around in diameter 6.5 µm for sample 210428 and between 2.8 and 3.5 µm in diameter for sample 210510. The fibres were around 2 µm in diameter for sample 210428 and around 1 µm in diameter for sample 210510. The electrospun fibres were cured in a UV-ozone cleaner in order increase the water stability. The method prevent full dissolution of the fibres, however the effect of curing in the centre of a fibre mat were questionable, as SEM images suggest dissolution of lower layers of fibres. Several 3D printed droplet generators were prototyped but the final droplet generator design were the dual droplet generator. The droplet generation within this device with the 20% PVP solution and GSO were performed for the two flow rate sets. The droplets produced for flow rate set 1 had diameters of 0.469 µm with a standard deviation of 0.213 µm. The droplet produced by flow rate set 2 had diameters of 0.742 µm with a standard deviation of 0.0159 µm. The same droplet generation were simulated in both 2D and 3D with COMSOL Multiphysics v5.5. The produced droplets had diameters around 1400 and 1550 µm for 2D and 3D, respectively.

Chapter 6

OUTLOOK

Further improvements of this project were considered and some suggestions towards this were made.

The release profiles obtained could have been triple determined in order verify the results obtained.

The PVP polymer did have some possible applications, however, a better crosslinking method should be investigated. Further investigation of different polymer systems could be conducted. The polymers tested in this project were only tested for one channel geometry. By changing the channel geometry emulsion electrospinning with different polymers could be possible.

The reliability of the 3D printed droplet generators could be tested, in order to ensure if inhomogeneities in the various droplet generators had any effect on the formed droplets.

3D printing of a mould which can be used to produce droplet generators with smaller channel sizes, could be feasible as exterior features have better resolution. This better resolution could enable moulding of channels around 200 µm in diameter.

The parameters regarding the COMSOL simulations could be determined in experimentally in order to improve the models.

BIBLIOGRAPHY

[1] I. Uslu, A. A. Serincay, and Halime, *Preparation of PVA/PAA/PEG/PVP Nanofibers with HPMC and Aloe Vera*, 2013.

[2] A. Arinstein, *Electrospun Polymer Nanofibers*. Singapore, SINGAPORE: Jenny Stanford Publishing, 2017, ISBN: 9789814745284.

[3] S. Ramakrishna, T.-C. Lim, K. Fujihara, W. E. Teo, and Z. Ma, *Introduction To Electrospinning And Nanofibers, An*. Singapore, SINGAPORE: World Scientific Publishing Company, 2005, ISBN: 9789812567611.

[4] I. D. Kim, A. Rothschild, B. H. Lee, D. Y. Kim, S. M. Jo, and H. L. Tuller, "Ultrasensitive chemiresistors based on electrospun TiO 2 nanofibers", *Nano Letters*, vol. 6, no. 9, pp. 2009–2013, Sep. 2006.

[5] Z. Zhang, X. Li, C. Wang, L. Wei, Y. Liu, and C. Shao, "ZnO hollow nanofibers: Fabrication from facile single capillary electrospinning and applications in gas sensors", *Journal of Physical Chemistry C*, vol. 113, no. 45, pp. 19 397–19 403, 2009.

[6] Y. Yu, L. Gu, C. Zhu, P. A. Van Aken, and J. Maier, "Tin nanoparticles encapsulated in porous multichannel carbon microtubes: Preparation by single-nozzle electrospinning and application as anode material for high-performance Li-based batteries", *Journal of the American Chemical Society*, vol. 131, no. 44, pp. 15 984–15 985, 2009.

[7] D. G. Yu, L. D. Gao, K. White, C. Branford-White, W. Y. Lu, and L. M. Zhu, "Multicomponent amorphous nanofibers electrospun from hot aqueous solutions of a poorly soluble drug", *Pharmaceutical Research*, vol. 27, no. 11, pp. 2466–2477, Nov. 2010.

[8] S. Sundarrajan and S. Ramakrishna, "Fabrication of nanocomposite membranes from nanofibers and nanoparticles for protection against chemical warfare stimulants", *Journal of Materials Science*, vol. 42, no. 20, pp. 8400–8407, Oct. 2007.

[9] O. Akhavan, *Graphene scaffolds in progressive nanotechnology/stem cell-based tissue engineering of the nervous system*, 2016.

[10] N. L. Lala, R. Ramaseshan, L. Bojun, S. Sundarrajan, R. S. Barhate, Y. J. Liu, and S. Ramakrishna, "Fabrication of nanofibers with antimicrobial functionality

used as filters: Protection against bacterial contaminants", *Biotechnology and Bioengineering*, vol. 97, no. 6, pp. 1357–1365, Aug. 2007.

[11] D. Lin, H. Wu, R. Zhang, and W. Pan, "Enhanced photocatalysis of electrospun Ag-ZnO heterostructured nanofibers", *Chemistry of Materials*, vol. 21, no. 15, pp. 3479–3484, Sep. 2009.

[12] M. M. Munir, H. Widiyandari, F. Iskandar, and K. Okuyama, "Patterned indium tin oxide nanofiber films and their electrical and optical performance", *Nanotechnology*, vol. 19, no. 37, Sep. 2008.

[13] S. Thenmozhi, N. Dharmaraj, K. Kadirvelu, and H. Y. Kim, *Electrospun nanofibers: New generation materials for advanced applications*, Mar. 2017.

[14] S. Mohammadzadehmoghadam, Y. Dong, S. Barbhuiya, L. Guo, D. Liu, R. Umer, X. Qi, and Y. Tang, "Electrospinning: Current Status and Future Trends", in *Nano-size Polymers: Preparation, Properties, Applications*, S. Fakirov, Ed. Springer International Publishing, 2016, pp. 89–154, ISBN: 978-3-319-39715-3.

[15] V. Pillay, C. Dott, Y. E. Choonara, C. Tyagi, L. Tomar, P. Kumar, L. C. Du Toit, and V. M. Ndesendo, *A review of the effect of processing variables on the fabrication of electrospun nanofibers for drug delivery applications*, 2013.

[16] E. Pinho and G. Soares, "Functionalization of cotton cellulose for improved wound healing", *Journal of Materials Chemistry B*, vol. 6, no. 13, pp. 1887–1898, 2018.

[17] A. Polini, S. Pagliara, R. Stabile, G. S. Netti, L. Roca, C. Prattichizzo, L. Gesualdo, R. Cingolani, and D. Pisignano, "Collagen-functionalised electrospun polymer fibers for bioengineering applications", *Soft Matter*, vol. 6, no. 8, pp. 1668–1674, 2010.

[18] J. Pelipenko, P. Kocbek, and J. Kristl, "Nanofiber diameter as a critical parameter affecting skin cell response", *European Journal of Pharmaceutical Sciences*, vol. 66, pp. 29–35, Jan. 2015.

[19] S. R. Gomes, G. Rodrigues, G. G. Martins, M. A. Roberto, M. Mafra, C. M. Henriques, and J. C. Silva, "In vitro and in vivo evaluation of electrospun nanofibers of PCL, chitosan and gelatin: A comparative study", *Materials Science and Engineering C*, vol. 46, pp. 348–358, Jan. 2015.

[20] S. P. Miguel, M. P. Ribeiro, P. Coutinho, and I. J. Correia, "Electrospun polycaprolactone/Aloe Vera_chitosan nanofibrous asymmetric membranes aimed for wound healing applications", *Polymers*, vol. 9, no. 5, 2017.

[21] X. Zong, S. Li, E. Chen, B. Garlick, K. S. Kim, D. Fang, J. Chiu, T. Zimmerman, C. Brathwaite, B. S. Hsiao, and B. Chu, "Prevention of postsurgery-induced

abdominal adhesions by electrospun bioabsorbable nanofibrous poly(lactide-co-glycolide)-based membranes", *Annals of Surgery*, vol. 240, no. 5, pp. 910–915, Nov. 2004.

[22] S. Agarwal, M. Burgard, A. Greiner, and J. Wendorff, *Electrospinning : A Practical Guide to Nanofibers*. Berlin/Boston, GERMANY: De Gruyter, Inc., 2016, ISBN: 9783110333510.

[23] B. Avinash and M. Yiu-Wing, "Functional Fibers Produced Using Electrospinning Techniques for Energy Scavenging Applications", in *Functional and Physical Properties of Polymer Nanocomposites*, John Wiley & Sons, Incorporated, 2016, pp. 45–47, ISBN: 9781118542293.

[24] D. Demir, A. Vaseashta, and N. Bölgen, "Recent Advances of Electrospinning and Multifunctional Electrospun Textile Materials for Chemical and Biological Protection", in *Nanoscience and Nanotechnology in Security and Protection against CBRN Threats*, P. Petkov, M. E. Achour, and C. Popov, Eds., Dordrecht: Springer Netherlands, 2020, pp. 275–289, ISBN: 978-94-024-2018-0.

[25] J. Xue, T. Wu, Y. Dai, and Y. Xia, *Electrospinning and electrospun nanofibers: Methods, materials, and applications*, Apr. 2019.

[26] G. Taylor, "Disintegration of Water Drops in an Electric Field", Tech. Rep. 1382, 1964, pp. 383–397.

[27] G. Taylor and M. D. Van Dyke, "Electrically driven jets With an appendix by", Tech. Rep., 1969, pp. 453–475.

[28] T. Han, D. H. Reneker, and A. L. Yarin, "Pendulum-like motion of straight electrified jets", *Polymer*, vol. 49, no. 8, pp. 2160–2169, Apr. 2008.

[29] G. Collins, J. Federici, Y. Imura, and L. H. Catalani, "Charge generation, charge transport, and residual charge in the electrospinning of polymers: A review of issues and complications", *Journal of Applied Physics*, vol. 111, no. 4, p. 44 701, Feb. 2012.

[30] L. H. Catalani, G. Collins, and M. Jaffe, "Evidence for molecular orientation and residual charge in the electrospinning of poly(butylene terephthalate) nanofibers", *Macromolecules*, vol. 40, no. 5, pp. 1693–1697, Mar. 2007.

[31] F. Liu, R. Guo, M. Shen, S. Wang, and X. Shi, "Effect of Processing Variables on the Morphology of Electrospun Poly[(lactic acid)- <i>co</i> -(glycolic acid)] Nanofibers", *Macromolecular Materials and Engineering*, vol. 294, no. 10, pp. 666–672, Oct. 2009.

[32] V. N. Morozov, T. Y. Morozova, and N. R. Kallenbach, “Atomic force microscopy of structures produced by electrospraying polymer solutions”, *International Journal of Mass Spectrometry*, vol. 178, no. 3, pp. 143–159, Nov. 1998.

[33] A. Balogh, R. Cselkó, B. Démuth, G. Verreck, J. Mensch, G. Marosi, and Z. K. Nagy, “Alternating current electrospinning for preparation of fibrous drug delivery systems”, *International Journal of Pharmaceutics*, vol. 495, no. 1, pp. 75–80, Nov. 2015.

[34] H. Niu and T. Lin, *Fiber generators in needleless electrospinning*, 2012.

[35] W. Tomaszewski and M. Szadkowski, “Investigation of Electrospinning with the Use of a Multi-jet Electrospinning Head”, Tech. Rep. 4.

[36] S. L. Liu, Y. Z. Long, Z. H. Zhang, H. D. Zhang, B. Sun, J. C. Zhang, and W. P. Han, “Assembly of oriented ultrafine polymer fibers by centrifugal electrospinning”, *Journal of Nanomaterials*, vol. 2013, 2013.

[37] D. Edmondson, A. Cooper, S. Jana, D. Wood, and M. Zhang, “Centrifugal electrospinning of highly aligned polymer nanofibers over a large area”, *Journal of Materials Chemistry*, vol. 22, no. 35, pp. 18 646–18 652, Sep. 2012.

[38] M. Kancheva, A. Toncheva, N. Manolova, and I. Rashkov, “Advanced centrifugal electrospinning setup”, *Materials Letters*, vol. 136, pp. 150–152, Dec. 2014.

[39] C. C. Liao, S. S. Hou, C. C. Wang, and C. Y. Chen, “Electrospinning fabrication of partially crystalline bisphenol A polycarbonate nanofibers: The effects of molecular motion and conformation in solutions”, *Polymer*, vol. 51, no. 13, pp. 2887–2896, Jun. 2010.

[40] P. McClellan and W. J. Landis, “Recent Applications of Coaxial and Emulsion Electrospinning Methods in the Field of Tissue Engineering”, *BioResearch Open Access*, vol. 5, no. 1, pp. 212–227, Aug. 2016.

[41] C. Y. Wang, J. J. Liu, C. Y. Fan, X. M. Mo, H. J. Ruan, and F. F. Li, “The effect of aligned core-shell nanofibres delivering NGF on the promotion of sciatic nerve regeneration”, *Journal of Biomaterials Science, Polymer Edition*, vol. 23, no. 1-4, pp. 167–184, 2012.

[42] P. Ducheyne, K. Healy, D. W. Hutmacher, D. W. Grainger, and C. J. Kirkpatrick, *Comprehensive Biomaterials II*. London, UNITED KINGDOM: Elsevier, 2017, pp. 528–544, ISBN: 9780081006924.

[43] M. F. Abdullah, T. Nuge, A. Andriyana, B. C. Ang, and F. Muhamad, *Core-Shell fibers: Design, roles, and controllable release strategies in tissue engineering and drug delivery*, Dec. 2019.

[44] L. E. Sperling, K. P. Reis, P. Pranke, and J. H. Wendorff, *Advantages and challenges offered by biofunctional core-shell fiber systems for tissue engineering and drug delivery*, Aug. 2016.

[45] G. Piccirillo, D. A. Carvajal Berrio, A. Laurita, A. Pepe, B. Bochicchio, K. Schenke-Layland, and S. Hinderer, “Controlled and tuneable drug release from electrospun fibers and a non-invasive approach for cytotoxicity testing”, *Scientific Reports*, vol. 9, no. 1, pp. 1–10, Dec. 2019.

[46] Q. Zhang, Y. Li, Z. Y. W. Lin, K. K. Wong, M. Lin, L. Yildirimer, and X. Zhao, *Electrospun polymeric micro/nanofibrous scaffolds for long-term drug release and their biomedical applications*, Sep. 2017.

[47] X. Li, Y. Su, S. Liu, L. Tan, X. Mo, and S. Ramakrishna, “Encapsulation of proteins in poly(l-lactide-co-caprolactone) fibers by emulsion electrospinning”, *Colloids and Surfaces B: Biointerfaces*, vol. 75, no. 2, pp. 418–424, Feb. 2010.

[48] S. Yan, L. Xiaoqiang, T. Lianjiang, H. Chen, and M. Xiumei, “Poly(l-lactide-co-ϵ-caprolactone) electrospun nanofibers for encapsulating and sustained releasing proteins”, *Polymer*, vol. 50, no. 17, pp. 4212–4219, Aug. 2009.

[49] Y. Zhang and H. Liu, “Physics of Multiphase Microflows and Microdroplets”, in *Microdroplet Technology*, Springer, 2012, ch. 1, pp. 1–21, ISBN: 978-1-4614-3264-7.

[50] P. Zhu and L. Wang, “Passive and active droplet generation with microfluidics: a review”, *Lab on a Chip*, vol. 17, 2017.

[51] S. Colin, “Introduction to Microflows”, in *Microfluidics*, John Wiley & Sons, Incorporated, 2013, ch. 1, pp. 1–23, ISBN: 9781848210974.

[52] R. Song, M. S. Abbasi, and J. Lee, “Fabrication of 3D printed modular microfluidic system for generating and manipulating complex emulsion droplets”, *Microfluidics and Nanofluidics*, vol. 23, no. 7, p. 92, Jul. 2019.

[53] G. F. Christopher and S. L. Anna, “Microfluidic methods for generating continuous droplet streams”, *Journal of Physics D: Applied Physics*, vol. 40, 2007.

[54] R. Seemann, M. Brinkmann, T. Pfohl, and S. Herminghaus, “Droplet based microfluidics”, *Reports on Progress in Physics*, vol. 75, 2011.

[55] G. T. Vladisavljević, R. A. Nuumani, and S. A. Nabavi, “Microfluidic Production of Multiple Emulsions”, *Micromachines*, vol. 8, 2017.

[56] T. Femmer, A. Jans, R. Eswein, N. Anwar, M. Moeller, M. Wessling, and A. J. C. Kuehne, “High-Throughput Generation of Emulsions and Microgels in Parallelized Microfluidic Drop-Makers Prepared by Rapid Prototyping”, 2015.

[57] J. L. Erkal, A. Selimovic, B. C. Gross, S. Y. Lockwood, E. L. Walton, S. McNamara, R. S. Martin, and D. M. Spence, “3D printed microfluidic devices with

integrated versatile and reusable electrodes", *Lab on a Chip*, vol. 14, no. 12, pp. 2023–2032, Jun. 2014.

[58] "An overview of additive manufacturing (3D printing) for microfabrication", *Microsystem Technologies*, vol. 23, no. 4, pp. 1117–1124, Apr. 2017.

[59] C. Chen, B. T. Mehl, A. S. Munshi, A. D. Townsend, D. M. Spence, and R. S. Martin, *3D-printed microfluidic devices: fabrication, advantages and limitations - a mini review*, Aug. 2016.

[60] J. Faria, C. Echeverria, J. P. Borges, M. H. Godinho, and P. I. Soares, "Towards the development of multifunctional hybrid fibrillary gels: Production and optimization by colloidal electrospinning", *RSC Advances*, vol. 7, no. 77, pp. 48 972–48 979, Oct. 2017.

[61] M. L. Bruschi, *Strategies to Modify the Drug Release from Pharmaceutical Systems.* Cambridge, UNITED KINGDOM: Elsevier Science & Technology, 2015, pp. 63–78, ISBN: 9780081001127.

[62] M. Nasari, D. Semnani, M. Hadjianfar, and S. Amanpour, "Poly (ϵ-caprolactone)/poly (N-vinyl-2-pyrrolidone) core–shell nanofibers loaded by multi-walled carbon nanotubes and 5-fluorouracil: an anticancer drug delivery system", *Journal of Materials Science*, vol. 55, no. 23, pp. 10 185–10 201, Aug. 2020.

[63] B. Ghafoor, A. Aleem, M. Najabat Ali, and M. Mir, *Review of the fabrication techniques and applications of polymeric electrospun nanofibers for drug delivery systems*, Dec. 2018.

[64] A. G. Gaonkar, "Interfacial tensions of vegetable oil/water systems: Effect of oil purification", *Journal of the American Oil Chemists' Society*, vol. 66, no. 8, pp. 1090–1092, Aug. 1989.

[65] K. Kowsari, B. Zhang, S. Panjwani, Z. Chen, H. Hingorani, S. Akbari, N. X. Fang, and Q. Ge, "Photopolymer formulation to minimize feature size, surface roughness, and stair-stepping in digital light processing-based three-dimensional printing", *Additive Manufacturing*, vol. 24, pp. 627–638, Dec. 2018.

[66] A. Luongo, V. Falster, M. B. Doest, M. M. Ribo, E. R. Eiriksson, D. B. Pedersen, and J. R. Frisvad, "Microstructure Control in 3D Printing with Digital Light Processing", *Computer Graphics Forum*, vol. 39, no. 1, pp. 347–359, Feb. 2019.

Appendix A

Reprint rights

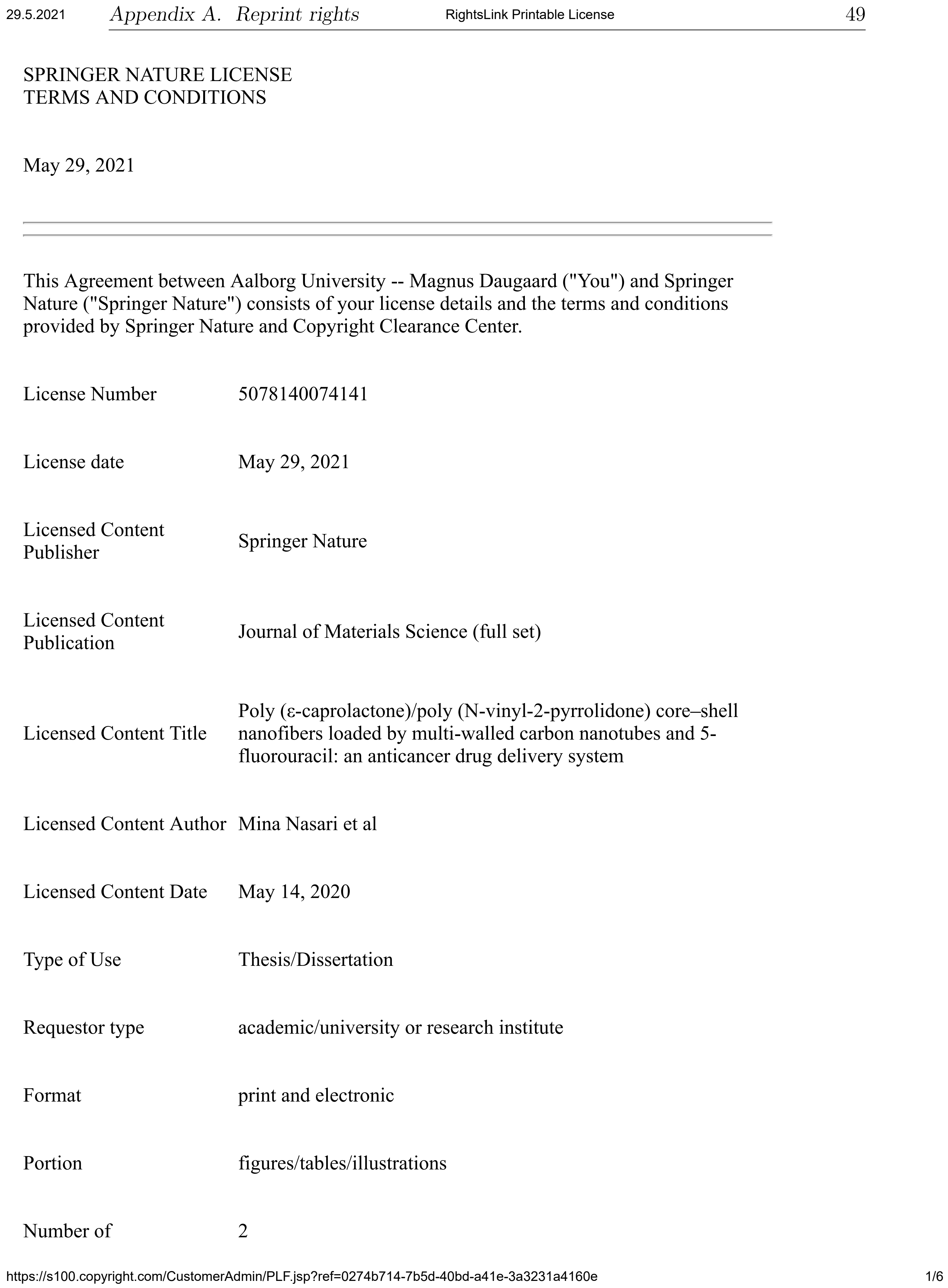

SPRINGER NATURE LICENSE
TERMS AND CONDITIONS

May 29, 2021

This Agreement between Aalborg University -- Magnus Daugaard ("You") and Springer Nature ("Springer Nature") consists of your license details and the terms and conditions provided by Springer Nature and Copyright Clearance Center.

License Number	5078140074141
License date	May 29, 2021
Licensed Content Publisher	Springer Nature
Licensed Content Publication	Journal of Materials Science (full set)
Licensed Content Title	Poly (ε-caprolactone)/poly (N-vinyl-2-pyrrolidone) core–shell nanofibers loaded by multi-walled carbon nanotubes and 5-fluorouracil: an anticancer drug delivery system
Licensed Content Author	Mina Nasari et al
Licensed Content Date	May 14, 2020
Type of Use	Thesis/Dissertation
Requestor type	academic/university or research institute
Format	print and electronic
Portion	figures/tables/illustrations
Number of	2

figures/tables/illustrations

Will you be translating?	no
Circulation/distribution	1 - 29
Author of this Springer Nature content	no
Title	Emulsion ElectrospinningAntibacterial Fibres with a 3D PrintedMicrofluidic Droplet Generator
Institution name	Aalborg University
Expected presentation date	Jun 2021
Portions	figure. 10
Requestor Location	Aalborg University Blåkildevej 11b 3,4 Aalborg Øst, Danmark 9220 Denmark Attn: Aalborg University
Total	0.00 EUR
Terms and Conditions	

Springer Nature Customer Service Centre GmbH
Terms and Conditions

This agreement sets out the terms and conditions of the licence (the **Licence**) between you and **Springer Nature Customer Service Centre GmbH** (the **Licensor**). By clicking 'accept' and completing the transaction for the material (**Licensed Material**), you also confirm your acceptance of these terms and conditions.

1. Grant of License

1. 1. The Licensor grants you a personal, non-exclusive, non-transferable, world-wide licence to reproduce the Licensed Material for the purpose specified in your order

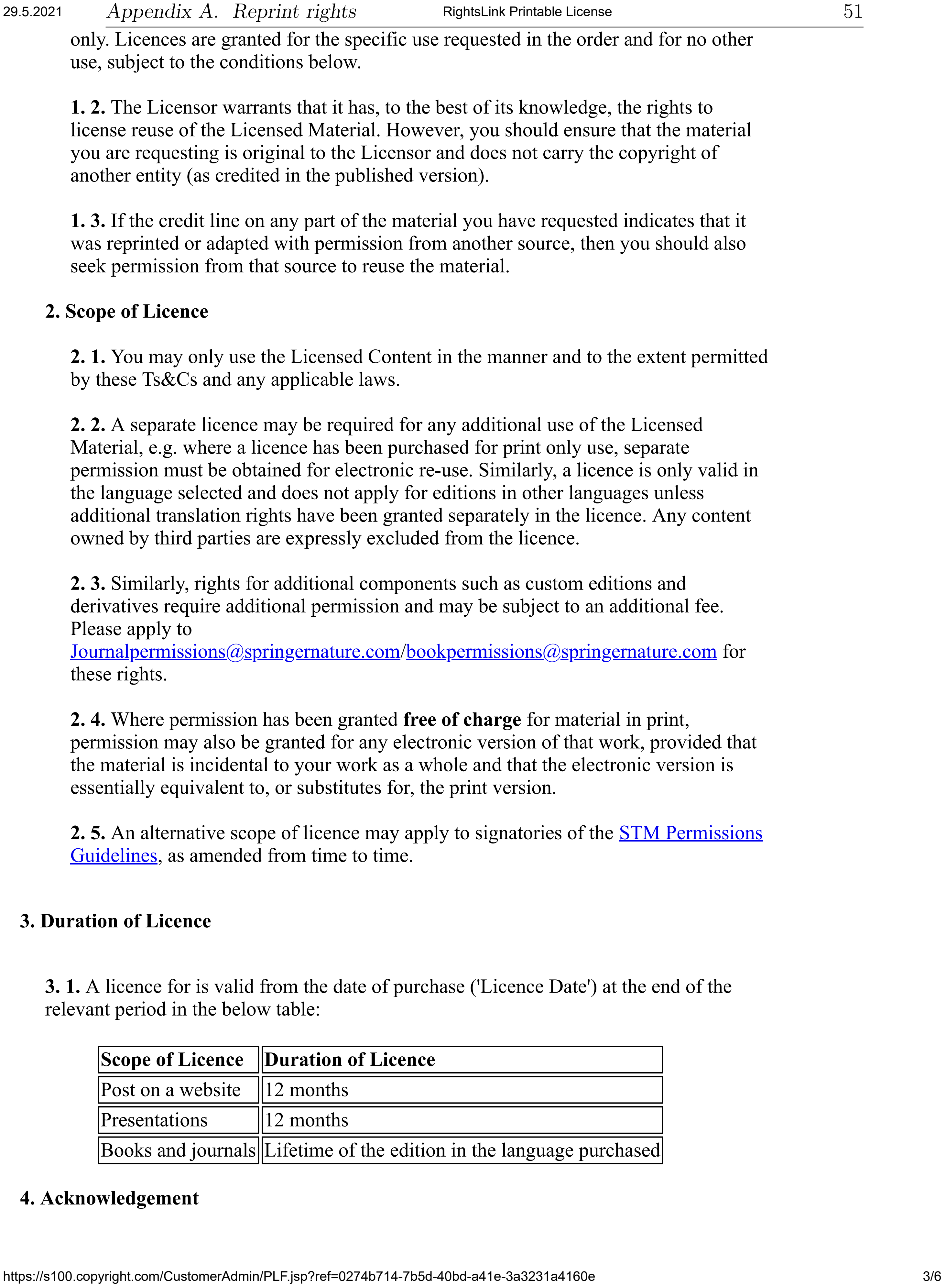

only. Licences are granted for the specific use requested in the order and for no other use, subject to the conditions below.

1. 2. The Licensor warrants that it has, to the best of its knowledge, the rights to license reuse of the Licensed Material. However, you should ensure that the material you are requesting is original to the Licensor and does not carry the copyright of another entity (as credited in the published version).

1. 3. If the credit line on any part of the material you have requested indicates that it was reprinted or adapted with permission from another source, then you should also seek permission from that source to reuse the material.

2. Scope of Licence

2. 1. You may only use the Licensed Content in the manner and to the extent permitted by these Ts&Cs and any applicable laws.

2. 2. A separate licence may be required for any additional use of the Licensed Material, e.g. where a licence has been purchased for print only use, separate permission must be obtained for electronic re-use. Similarly, a licence is only valid in the language selected and does not apply for editions in other languages unless additional translation rights have been granted separately in the licence. Any content owned by third parties are expressly excluded from the licence.

2. 3. Similarly, rights for additional components such as custom editions and derivatives require additional permission and may be subject to an additional fee. Please apply to Journalpermissions@springernature.com/bookpermissions@springernature.com for these rights.

2. 4. Where permission has been granted **free of charge** for material in print, permission may also be granted for any electronic version of that work, provided that the material is incidental to your work as a whole and that the electronic version is essentially equivalent to, or substitutes for, the print version.

2. 5. An alternative scope of licence may apply to signatories of the STM Permissions Guidelines, as amended from time to time.

3. Duration of Licence

3. 1. A licence for is valid from the date of purchase ('Licence Date') at the end of the relevant period in the below table:

Scope of Licence	**Duration of Licence**
Post on a website	12 months
Presentations	12 months
Books and journals	Lifetime of the edition in the language purchased

4. Acknowledgement

4. 1. The Licensor's permission must be acknowledged next to the Licenced Material in print. In electronic form, this acknowledgement must be visible at the same time as the figures/tables/illustrations or abstract, and must be hyperlinked to the journal/book's homepage. Our required acknowledgement format is in the Appendix below.

5. Restrictions on use

5. 1. Use of the Licensed Material may be permitted for incidental promotional use and minor editing privileges e.g. minor adaptations of single figures, changes of format, colour and/or style where the adaptation is credited as set out in Appendix 1 below. Any other changes including but not limited to, cropping, adapting, omitting material that affect the meaning, intention or moral rights of the author are strictly prohibited.

5. 2. You must not use any Licensed Material as part of any design or trademark.

5. 3. Licensed Material may be used in Open Access Publications (OAP) before publication by Springer Nature, but any Licensed Material must be removed from OAP sites prior to final publication.

6. Ownership of Rights

6. 1. Licensed Material remains the property of either Licensor or the relevant third party and any rights not explicitly granted herein are expressly reserved.

7. Warranty

IN NO EVENT SHALL LICENSOR BE LIABLE TO YOU OR ANY OTHER PARTY OR ANY OTHER PERSON OR FOR ANY SPECIAL, CONSEQUENTIAL, INCIDENTAL OR INDIRECT DAMAGES, HOWEVER CAUSED, ARISING OUT OF OR IN CONNECTION WITH THE DOWNLOADING, VIEWING OR USE OF THE MATERIALS REGARDLESS OF THE FORM OF ACTION, WHETHER FOR BREACH OF CONTRACT, BREACH OF WARRANTY, TORT, NEGLIGENCE, INFRINGEMENT OR OTHERWISE (INCLUDING, WITHOUT LIMITATION, DAMAGES BASED ON LOSS OF PROFITS, DATA, FILES, USE, BUSINESS OPPORTUNITY OR CLAIMS OF THIRD PARTIES), AND
WHETHER OR NOT THE PARTY HAS BEEN ADVISED OF THE POSSIBILITY OF SUCH DAMAGES. THIS LIMITATION SHALL APPLY NOTWITHSTANDING ANY FAILURE OF ESSENTIAL PURPOSE OF ANY LIMITED REMEDY PROVIDED HEREIN.

8. Limitations

8. 1. ***BOOKS ONLY:***Where **'reuse in a dissertation/thesis'** has been selected the following terms apply: Print rights of the final author's accepted manuscript (for clarity, NOT the published version) for up to 100 copies, electronic rights for use only on a personal website or institutional repository as defined by the Sherpa guideline (www.sherpa.ac.uk/romeo/).

8. 2. For content reuse requests that qualify for permission under the STM Permissions Guidelines, which may be updated from time to time, the STM Permissions Guidelines supersede the terms and conditions contained in this licence.

9. Termination and Cancellation

9. 1. Licences will expire after the period shown in Clause 3 (above).

9. 2. Licensee reserves the right to terminate the Licence in the event that payment is not received in full or if there has been a breach of this agreement by you.

Appendix 1 — Acknowledgements:

For Journal Content:
Reprinted by permission from [**the Licensor**]: [**Journal Publisher** (e.g. Nature/Springer/Palgrave)] [**JOURNAL NAME**] [**REFERENCE CITATION** (Article name, Author(s) Name), [**COPYRIGHT**] (year of publication)

For **Advance Online Publication papers:**
Reprinted by permission from [**the Licensor**]: [**Journal Publisher** (e.g. Nature/Springer/Palgrave)] [**JOURNAL NAME**] [**REFERENCE CITATION** (Article name, Author(s) Name), [**COPYRIGHT**] (year of publication), advance online publication, day month year (doi: 10.1038/sj.[JOURNAL ACRONYM].)

For Adaptations/Translations:
Adapted/Translated by permission from [**the Licensor**]: [**Journal Publisher** (e.g. Nature/Springer/Palgrave)] [**JOURNAL NAME**] [**REFERENCE CITATION** (Article name, Author(s) Name), [**COPYRIGHT**] (year of publication)

Note: For any republication from the British Journal of Cancer, the following credit line style applies:

Reprinted/adapted/translated by permission from [**the Licensor**]: on behalf of Cancer Research UK: : [**Journal Publisher** (e.g. Nature/Springer/Palgrave)] [**JOURNAL NAME**] [**REFERENCE CITATION** (Article name, Author(s) Name), **[COPYRIGHT]** (year of publication)

For **Advance Online Publication** papers:
Reprinted by permission from The [**the Licensor**]: on behalf of Cancer Research UK: [**Journal Publisher** (e.g. Nature/Springer/Palgrave)] [**JOURNAL NAME**] [**REFERENCE CITATION** (Article name, Author(s) Name), [**COPYRIGHT**] (year of publication), advance online publication, day month year (doi: 10.1038/sj. [JOURNAL ACRONYM])

For Book content:
Reprinted/adapted by permission from [**the Licensor**]: [**Book Publisher** (e.g. Palgrave Macmillan, Springer etc) [**Book Title**] by [**Book author**(s)] [**COPYRIGHT**] (year of publication)

Other Conditions:

Version 1.3

Questions? customercare@copyright.com or +1-855-239-3415 (toll free in the US) or +1-978-646-2777.